ISTANBUL TECHNICAL UNIVERSITY ★ GRADUATE SCHOOL

TESTING SPATIAL CURVATURE AND ANISOTROPIC EXPANSION OF THE UNIVERSE ON TOP OF THE ΛCDM MODEL

M.Sc. THESIS

Maya ÖZYİĞİT

Department of Physics Engineering

Physics Engineering Programme

OCTOBER 2022

ISTANBUL TECHNICAL UNIVERSITY ★ GRADUATE SCHOOL

TESTING SPATIAL CURVATURE AND ANISOTROPIC EXPANSION OF THE UNIVERSE ON TOP OF THE ΛCDM MODEL

M.Sc. THESIS

Maya ÖZYİĞİT
(509191126)

Department of Physics Engineering

Physics Engineering Programme

Thesis Advisor: Assoc. Prof. Dr. Özgür AKARSU

OCTOBER 2022

İSTANBUL TEKNİK ÜNİVERSİTESİ ★ LİSANSÜSTÜ EĞİTİM ENSTİTÜSÜ

ΛCDM MODELİ ÜZERİNE EVRENİN UZAYSAL EĞRİLİĞİNİN VE GENİŞLEME YÖNBAĞIMLILIĞININ SINANMASI

YÜKSEK LİSANS TEZİ

Maya ÖZYİĞİT
(509191126)

Fizik Mühendisliği Anabilim Dalı

Fizik Mühendisliği Programı

Tez Danışmanı: Doç. Dr. Özgür AKARSU

EKİM 2022

Maya ÖZYİĞİT, a M.Sc. student of ITU Graduate School student ID 509191126, successfully defended the thesis entitled "TESTING SPATIAL CURVATURE AND ANISOTROPIC EXPANSION OF THE UNIVERSE ON TOP OF THE ΛCDM MODEL", which she prepared after fulfilling the requirements specified in the associated legislations, before the jury whose signatures are below.

Thesis Advisor :	**Assoc. Prof. Dr. Özgür AKARSU** Istanbul Technical University	....
Jury Members :	**Prof. Dr. A. Savaş Arapoğlu** Istanbul Technical University	....
	Assoc. Prof. Dr. Nihan Katırcı Doğuş University	....

Date of Submission : 11 October 2022
Date of Defense : 24 October 2022

To my family,

FOREWORD

I would like to express my sincere gratitude to my thesis advisor Assoc. Prof. Dr. Özgür Akarsu for his guidance, immense knowledge, and continuous support throughout this study, without whom this work would not be possible. Special thanks to Dr. Eleonora Di Valentino, Prof. Dr. Suresh Kumar, and Asst. Prof. Dr. Shivani Sharma whom I have collaborated with.

Lastly, I would like to thank my mother for her endless support and all she has done.

October 2022 Maya ÖZYİĞİT

TABLE OF CONTENTS

Page

ABBREVIATIONS

ΛCDM	: Lambda Cold Dark Matter
FLRW	: Friedmann Lemaitre Robertson Walker
RW	: Robertson Walker
GR	: General Relativity
CMB	: Cosmic Microwave Background
WMAP	: Wilkinson Microwave Anisotropy Probe
BAO	: Baryon Acoustic Oscillation
CC	: Cosmic Chronometers
SNIa	: Type Ia Supernovae
HST	: Hubble Space Telescope
Mpc	: Megaparsec
SH0ES	: Supernova H_0 for the Equation of State
km	: Kilometer
s	: Second
BBN	: Big Bang Nucleosynthesis
EMT	: Energy-Momentum Tensor
EFE	: Einstein Field Equations
EMT	: Energy-Momentum Tensor
FIRAS	: The Far Infrared Absolute Spectrophotomete
EoS	: Equation of State
An-ΛCDM	: Anisotropic Lambda Cold Dark Matter
SDSS	: Sloan Digital Sky Survey
BOSS	: Baryon Oscillation Spectroscopic Survey
Lyα	: Lyman-α
eBOSS	: Extended Baryon Oscillation Spectroscopic Survey
MGS	: Main Galaxy Sample
ELG	: Emission Line Galaxies
LRG	: Luminous Red Galaxies
SNLS	: SuperNova Legacy Survey
PS1	: Pan-STARRS1
CL	: Confidence Level
LRS	: Locally Rotationally Symmetric
Pan	: Pantheon

SYMBOLS

$\boldsymbol{\Lambda}$	: Cosmological constant
$\boldsymbol{\rho}$	: Energy density
$\boldsymbol{p}$	: Pressure
$\boldsymbol{G_{\mu\nu}}$	: Einstein tensor
$\boldsymbol{G}$	: Newton's constant
$\boldsymbol{\Gamma^{\mu}_{\nu\sigma}}$	: Christoffel Symbols
$\boldsymbol{R_{\mu\nu}}$	: Ricci tensor
$\boldsymbol{R}$	: Ricci scalar
$\boldsymbol{T_{\mu\nu}}$	: Energy-momentum tensor
${}^3R$	: 3-Ricci scalar
$\boldsymbol{\sigma}^2$	: Shear scalar
$\boldsymbol{\sigma_{\alpha\beta}}$	: Shear tensor
$\boldsymbol{h_{\mu\nu}}$	: Projection tensor
$\boldsymbol{g_{\mu\nu}}$	: Metric tensor
$\boldsymbol{a},\boldsymbol{b},\boldsymbol{c}$	: Directional scale factors
$\boldsymbol{s}$	: Average expansion scale factor
$\boldsymbol{H}$	: Hubble parameter
$\boldsymbol{H_0}$	: Hubble constant
$\boldsymbol{h}$	: Dimensionless reduced Hubble constant
$\boldsymbol{\Omega}$	: Density parameter
$\boldsymbol{\nabla}$	: Covariant derivative
$\boldsymbol{T}$	: Temperature
$\boldsymbol{N_{\mathrm{eff}}}$	: Effective number of neutrino species
$\boldsymbol{\theta}$	: Angular scale
$\boldsymbol{u_{\mu}}$	: Four-velocity
$\boldsymbol{\Theta}$	: Volume expansion rate
$\boldsymbol{D^{\mu}}$	: Fully orthogonally projected covariant derivative
$\boldsymbol{m}$	: Mass
$\boldsymbol{c}$	: Speed of light
$\boldsymbol{c_{\mathrm{s}}}$	: Sound speed of the baryon fluid
$\boldsymbol{r_{\mathrm{s}}}$	: The comoving size of the sound horizon
$\boldsymbol{z}$	: Redshift
$\boldsymbol{t}$	: Cosmic (proper) time
$\boldsymbol{\chi^2}$	: Chi-squared function
$\mathcal{M}$	: Nuisance parameter
$\boldsymbol{C}$	: Covariance matrix
$\boldsymbol{D}$	: Diagonal covariance matrix

$\boldsymbol{\omega}_{\mathbf{b}}$	: Dimensionless present-day density of baryons
$\boldsymbol{\omega}_{\mathbf{cdm}}$	: Dimensionless present-day density of cold dark matter
$\boldsymbol{D}_L$	: Luminosity distance
$\boldsymbol{D}_H$	: Hubble distance
$\boldsymbol{D}_M$	: The comoving angular diameter distance
$\boldsymbol{D}_C$	: The comoving distance of the line-of-sight
$\boldsymbol{D}_V$	: The spherically averaged distance
$\mathcal{M}$	: Model
$\boldsymbol{P}$	: Posterior probabilities of the model
$\boldsymbol{D}$	: Data
$\mathcal{L}$	: Likelihood function
$\mathcal{E}$	: Bayesian Evidence
$\boldsymbol{B}$	: Bayes' factor

LIST OF TABLES

Page

LIST OF FIGURES

Page

TESTING SPATIAL CURVATURE AND ANISOTROPIC EXPANSION OF THE UNIVERSE ON TOP OF THE ΛCDM MODEL

SUMMARY

In this thesis, we explore the possible advantages of extending the standard ΛCDM model by more realistic backgrounds compared to its spatially flat Robertson-Walker (RW) spacetime assumption, while preserving the underpinning physics; in particular, by simultaneously allowing non-zero spatial curvature and anisotropic expansion on top of ΛCDM, viz., the An-*o*ΛCDM model. This is to test whether the latest observational data still support spatial flatness and/or isotropic expansion in this case, and, if not, to explore the roles of spatial curvature and expansion anisotropy (due to its stiff fluid-like behavior) in addressing some of the current cosmological tensions associated with ΛCDM. We first present the theoretical background and explicit mathematical construction of An-*o*ΛCDM. We replace, in the simplest manner, the spatially flat RW spacetime assumption of the ΛCDM model with the simplest more realistic background that simultaneously allows non-zero spatial curvature and anisotropic expansion; namely, considered the simplest anisotropic generalizations of the RW spacetime, viz., the Bianchi type I, V, and IX spacetimes (having the simplest homogeneous and flat, open, and closed spatial sections, respectively) combined in one Friedmann equation. Then we constrain the parameters of this model and its particular cases, namely, An-ΛCDM (allowing anisotropic expansion), *o*ΛCDM (allowing non-zero spatial curvature), and ΛCDM, by using the latest data sets from different observational probes, viz., Planck CMB(+Lens), BAO, SnIa Pantheon, and CC data, and discuss the results in detail. Ultimately, we conclude that, within the setup under consideration, (i) the observational data confirm the spatial flatness and isotropic expansion assumptions of ΛCDM, though a very small amount of expansion anisotropy cannot be excluded, e.g., $\Omega_{\sigma 0} \lesssim 10^{-18}$ (95% C.L.) for An-ΛCDM from CMB+Lens data, (ii) the introduction of spatial curvature or anisotropic expansion, or both, on top ΛCDM does not offer a possible relaxation to the H_0 tension, and (iii) the introduction of anisotropic expansion neither affects the closed space prediction from the CMB(+Lens) data nor does it improve the drastically reduced value of H_0 led by the closed space.

ΛCDM MODELİ ÜZERİNE EVRENİN UZAYSAL EĞRİLİĞİNİN VE GENİŞLEME YÖNBAĞIMLILIĞININ SINANMASI

ÖZET

Bu tezde, Lambda-Soğuk Karanlık Madde (ΛCDM) modeli olarak da bilinen standart kozmolojik modelin yalnızca uzaysal geometrisinin genelleştirilmesinin ayrıntılı bir kuramsal ve gözlemsel incelemesi sunulmuştur. ΛCDM modeli uzaysal olarak türdeş ve yönbağımsız düz Robertson-Walker (RW) uzayzaman metriği üzerine kuruludur. RW metriğinin yalnızca uzaysal yönbağımsızlığı ve düzlüğünün gevşetilmesiyle, uzaysal olarak türdeş ancak yönbağımlı ve eğri metrikler elde edilebilir ki, bu da ΛCDM modelinin temelini oluşturan genel görelilik, standart parçacık fiziği gibi yerleşik fizik yasalarını değiştirmeden daha gerçekçi evren modellerinin kurulmasına olanak sağlar. Buna göre, bu tez kapsamında uzaysal olarak türdeş ve yönbağımsız düz RW metriği, uzaysal olarak türdeş ancak başka eğrilik durumlarına sahip ve yönbağımlı Bianchi tip I, Bianchi tip V ve Bianchi tip IX uzayzaman metrikleriyle değiştirilmiş ve bunlar tek bir Friedmann denklemi altında toplanarak yönbağımlı ve başka uzaysal eğrilik durumlarına izin veren An-$o\Lambda$CDM kozmolojik modeli kurulmuştur. An-$o\Lambda$CDM modelinde ΛCDM modeline ek olarak yönbağımlı genişlemeden ve uzaysal eğrilikten gelen iki yeni geometrik parametre kuramsal ve gözlemsel olarak incelenmiştir. Standart ΛCDM modelinin yalnızca geometrik genelleştirmesi olarak kurduğumuz ve An-$o\Lambda$CDM adını verdiğimiz bu modelin, öncelikle, kuramsal olarak bazı güncel kozmojik problemlere yanıt olabilecek özelliklere sahip olup olmadığı kuramsal olarak ayrıntılı bir biçimde tartışılmış ve, sonra, değerleri iyi bilinen bazı kozmolojik parametreler ve yüksek duyarlıklı en son gözlemsel veriler dikkate alınarak kısıtlanmıştır; böylece günümüz evrenini anlatmakta RW metriğinin yeterli olup olamadığı da tartışılmıştır.

Tezde öncelikle, Bölüm 1'de, bilimsel araştırma konusu olarak standart ΛCDM modelinin geometrik bir genelleştirmesinin seçilmesinin gerekçesi verilmiştir. Bölüm 2'de, yönbağımlı ve başka uzaysal eğrilik durumlarına izin veren An-$o\Lambda$CDM modeli kurulmuştur. Öncelikle, uzaysal olarak türdeş ancak yönbağımlı ve başka eğrilik durumlarına sahip Bianchi tip I, Bianchi tip V ve Bianchi tip IX uzayzaman metrikleri incelenmiştir. Burada Bianchi tip I metriğinin özel durum olarak uzaysal olarak düz RW metriğini, Bianchi tip V metriğinin özel durum olarak uzaysal olarak açık RW metriğini ve Bianchi tip IX metriğinin özel durum olarak uzaysal olarak kapalı RW metriğini içerdiği gösterilmiştir. Bu metrikler çerçevesinde evrenin fiziksel içeriği mükemmel akışkan kabul edilerek ve bilindik bazı fiziksel kaynaklar (toz, ışınım, vakum) kullanılarak Einstein alan denklemleri çözülmüştür. Bianchi metrikleri uzayın üç yönde ayrı hızlarla evrimleşmesine izin verebildiğinden RW metriği çerçevesinde tanımlanan bazı kozmolojik parametreler genelleştirilerek bazı yeni büyüklükler

tanımlanmıştır: **(i)** Makaslama skaleri σ^2, uzaysal olarak yönbağımlı modellerde genişleme hızının farklı yönlerde farklı olmasının ölçüsüdür. **(ii)** Ortalama ölçek çarpanı s, birçok denklemin daha kolayca yazılmasını sağlayan bir parametredir. Daha sonra, Bianchi tip I, Bianchi tip V ve Bianchi tip IX uzayzamanları bir arada kullanılarak tek bir genel Friedmann denklemi, $H^2(s)/H_0^2 = \Omega_{\sigma 0}s^{-6} + \Omega_{\rm r0}s^{-4} + \Omega_{\rm m0}s^{-3} + \Omega_{\kappa 0}s^{-2} + \Omega_{\Lambda 0}$, yazılmıştır. An-$o\Lambda$CDM olarak adlandırdığımız bu modelde yönbağımlılıktan kaynaklanan makaslama skalerine karşılık gelen bir yoğunluk parametresinin bugünkü değeri, $\Omega_{\sigma 0}$, ve uzaysal eğriliğe karşılık gelen bir yoğunluk parametresinin bugünkü değeri, $\Omega_{\kappa 0}$, ΛCDM modeline ait Friedmann denkleminin üzerine yeni iki geometrik parametre olarak gelmiştir. Burada $\Omega_{\sigma 0}$ eksili değer almayan bir parametredir, $\Omega_{\kappa 0}$ ise sırasıyla uzaysal olarak düz, açık ve kapalı evrenlere karşılık gelen $\Omega_{\kappa 0} = 0$, $\Omega_{\kappa 0} > 0$, ve $\Omega_{\kappa 0} < 0$ değerlerini alabilir. Bölüm 3'te, gözlemsel çözümlemeleri gerçekleştirmek için kullanılan veri kümeleri; kozmik kronometreler (CC), tip Ia süpernovalar (SnIa Pantheon 2018), baryon yankılanım salınımları (BAO), kozmik ardalan ışınımı (CMB) ve kullanılan yöntem ayrıntılı bir biçimde anlatılmıştır. Gözlemsel kısıtlama sonuçlarına ayrılmış Bölüm 4'te, An-$o\Lambda$CDM modelinin ve bu modelin özel durumları olan An-ΛCDM (ΛCDM üzerine yalnızca yönbağımlı genişlemeyi serbest bırakan), $o\Lambda$CDM (ΛCDM üzerine yalnızca uzaysal eğriliği serbest bırakan) ve standart ΛCDM modelleri en güncel gözlemsel veri kümeleri kullanılarak kısıtlanmış ve kozmolojik açıdan önemli olan H_0, $\Omega_{\rm m0}$, $\Omega_{\kappa 0}$ ve $\Omega_{\sigma 0}$ parametreleri üzerine olan kısıtlar dahil olmak üzere tüm modellerin parametrelerine ait kısılara ilişkin sonuçlar 68% ve 95% güven aralığında verilmiştir. Modellerin parametreleri öncelikle düşük kırmızıya kayma değerlerinden gelen CC veri kümesi, Pan veri kümesi ve bileşik CC+Pan veri kümesi kullanılarak ayrı ayrı kısıtlanmıştır. Bu veri kümelerine bakıldığında uzaysal eğriliği içeren An-$o\Lambda$CDM ve $o\Lambda$CDM modelleri uzaysal olarak düz olan bir evreni desteklemektedir. Bu veri kümeleri için modellerin kestirdiği Hubble Sabiti (H_0) değerlerinde dikkate değer bir fark görülmemiştir; ancak, CC veri kümesi için yönbağımlı genişlemenin eklenmesinin kestirilen H_0 değerini arttırdığı, Pan veri kümesi için ise azalttığı görülmüştür. Düşük kırmızıya kayma değerlerinden gelen bu veri kümelerine bakıldığında genişleme yönbağımlılığı yoğunluk parametresi üzerine yapılan en iyi kısıtlama CC veri kümesinden $\Omega_{\sigma 0} < 10^{-2.23}$ olarak bulunmuş ve bu değerin modelden bağımsız SNIa ölçümlerinden gelen $\Omega_{\sigma 0} \lesssim 10^{-3}$ değerinden bir mertebe daha gevşek olduğu görülmüştür. Yönbağımlı genişlemenin dahil edilmesinden bağımsız olarak, CC veri kümesinin H_0 değeri üzerindeki kısıtlamasının $\Omega_{\kappa 0}$ değerine göre daha iyi olduğu, Pan veri kümesine bakıldığında ise $\Omega_{\kappa 0}$ değeri üzerindeki kısıtlamasının H_0 değerine göre daha iyi olduğu görülmüştür. Daha sonra modellerin bütün parametre uzayı BAO+Pan bileşik veri kümesi, CMB veri kümesi ve CMB+Pan bileşik veri kümesi kullanılarak kısıtlanmıştır. BAO verisi ile Pan verisi birlikte ele alındığında yönbağımlı genişlemenin yoğunluk parametresi üzerindeki kısıtlama iyileşerek $\Omega_{\sigma 0} \lesssim 10^{-14}$ değerini aldığı görülmüştür. BAO+Pan bileşik veri kümesinden H_0 ve $\Omega_{\kappa 0}$ değerleri arasında eksili bir ilişki gözlemlenmiştir; $\Omega_{\kappa 0}$ aldığı artılı değerlerde H_0 değeri daha küçük olmaktadır. CMB veri kümesine bakıldığında, ΛCDM modelinin Hubble sabiti için öngördüğü değer ile yerel ölçümlerden elde edilen H_0 değeri arasında gerilim gözlemlenmiştir. ΛCDM modelinin Hubble sabiti için öngördüğü değer $H_0 = 67.59 \pm 0.65$ km s^{-1} Mpc^{-1} iken SH0ES verilerinin öngördüğü değere $H_0 = 73.04 \pm 1.04$ km s^{-1} Mpc^{-1} bakıldığında bu gerilimin 5σ değerine kadar çıktığı görülmüştür. $o\Lambda$CDM modeline bakıldığında uzaysal eğriliğin de eklenmesiyle birlikte bu gerilimin, kapalı uzaysal eğrilik yönünde 3σ seviyesinde, arttığı görülmüştür. Pan veri kümesinin CMB veri kümesine eklendiğinde parametreler arasındaki bağlılaşımı kopararak parametre değerleri üzerinde daha iyi kısıtlamalar sağladığı gözlemlenmiştir. Bileşik CMB+Pan veri kümesinde An-ΛCDM ve ΛCDM modellerine uzaysal eğriliğin eklenmesi, $\Omega_{\kappa 0}$ değeri bu kümede iyi kısıtlandığından ve bu kısıtlama da uzaysal olarak düz bir evreni desteklediğinden, dikkate değer bir değişiklik getirmemiştir. Son olarak, modellerin günümüz yoğunluk parametreleri, öncelikle yüksek kırmızıya kayma değerlerinden gelen CMB+Lens ve CMB+Lens+BAO bileşik veri kümeleri kullanılarak, daha sonra da bu bileşik veri kümelerine düşük kırmızıya kayma değerlerinden gelen astrofiziksel veri kümeleri de eklenilerek CMB+Lens+Pan, CMB+Lens+BAO+Pan ve CMB+Lens+BAO+Pan+CC bileşik veri kümeleriyle kısıtlanmıştır. Yüksek ve düşük kırmızıya kayma değerlerinden gelen gözlemsel verilere ve bunların çeşitli kombinasyonlarına bakıldığında ΛCDM ve $o\Lambda$CDM modellerinin öngörülen günümüz yoğunluk parametrelerinin Planck 2018 sonuçlarıyla uyumlu olduğu ve yönbağımlı genişleme parametresi dahil edildiğinde sonuçların değişmediği gözlemlenmiştir. Bütün veri kümeleri için H_0 ve $\Omega_{\kappa 0}$ değerleri arasında artılı bir ilişki gözlemlenmiştir; $\Omega_{\kappa 0}$ aldığı eksili değerlere bağlı olarak H_0 değerinin de küçülme eğiliminde olduğu görülmüştür. Genişleme yönbağımlılığının günümüz yoğunluk parametresi üzerine yapılan en iyi kısıtlama CMB+Lens bileşik veri kümesinden $\Omega_{\sigma 0} \lesssim 10^{-18}$ olarak bulunmuş ve başka veri kümeleri için bu üst sınırda dikkate değer bir değişim gözlemlenmemiştir. Yönbağımlı genişlemenin modele eklenmesinin bu sonuçları değiştirmediği ve H_0 değerinde dikkate değer bir değişime neden olmadığı görülmüştür. ΛCDM modeline ek geometrik parametreler olarak gelen genişleme yönbağımlılığı ve uzaysal eğrilik literatürde standart ΛCDM modelinde ortaya çıkan Hubble Sabiti Problemi'ne çözüm sağlayamadığı görülmüştür. Son olarak, bölüm 5'te, bu tez kapsamında yürütülen bilimsel araştırmadan elde edilen dikkate değer kuramsal ve gözlemsel sonuçlar özetlenmiştir: **(i)** Güncel gözemsel veri kümelerinden elde edilen sonuçlar, ΛCDM modelinin uzayın düz, türdeş ve yönbağımsız bir geometriye sahip olduğu öngörüsünü desteklemektedir, ancak geç evrende bir ölçüde yönbağımlılığın ($\Omega_{\sigma 0} \lesssim 10^{-18}$) olabileceği yadsınamaz. **(ii)** ΛCDM modeline ek geometrik parametreler olarak gelen genişleme yönbağımlılığı ve/veya uzaysal eğrilik literatürde standart ΛCDM modelinde ortaya çıkan Hubble Sabiti Problemi'ne çözüm sağlayamamaktadır. **(iii)** ΛCDM modeline ek parametre olarak giren yönbağımlı genişlemenin, CMB veri kümesi çözümlemelerinin evrenin kapalı uzaysal eğriliğe sahip olduğu öngörüsünü etkilemediği ve kapalı uzaysal eğriliğin yol açtığı, öngörülen H_0 değerindeki düşüklük için bir iyileştirme sağlamadığı gözlemlenmiştir. Standart ΛCDM modelinin yalnızca geometrik genelleştirilmesi olarak kurulan An-$o\Lambda$CDM modeli, gözlemsel veriler karşısında standart ΛCDM modelinden daha başarılı olamamıştır.

1. INTRODUCTION

The work presented in this thesis is based on the joint work [1], in collaboration with Özgür Akarsu, Eleonora Di Valentino, Suresh Kumar and Shivani Sharma.

In the past decades, the scenario assumed as the standard model in cosmology is the so called Lambda cold dark matter (ΛCDM). This scenario fits a wide range of observational data on different scales and epochs of the universe [2–6]. However, some discrepancies and inconsistencies in the estimated values of some important cosmological parameters have emerged in the last decade [7–12]. These tensions, even if present with different statistical significance, and possibly due in part to systematic errors in the experiments, demand an explanation. Among all the possibilities, the necessity of physics beyond the well established fundamental theories that underpin, and even extend ΛCDM, is making its own way. Alternatively, it would be interesting to leave the physics completely untouched, and proceed by considering more realistic spacetimes compared to the spatially flat Friedmann-Lemaître-Robertson-Walker (FLRW) spacetime on which ΛCDM is established.

Here we explore the possible advantages of a pure geometric generalization of the standard ΛCDM model, in particular, allowing non-flat and anisotropic space. The standard ΛCDM model, relying on canonical inflationary paradigm [13–16], assumes a flat and, in accordance with the cosmological principle, maximally symmetric (homogeneous and isotropic) space, i.e., the spatially flat Robertson-Walker (RW) spacetime, for describing the geometry of the universe on the largest scales, and general relativity (GR) with a positive cosmological constant for describing the dynamics of the universe depending on its material content. It is important to investigate whether these geometric assumptions would still be favored by the latest observational data when the spatially flat RW spacetime is generalized to a more realistic one. Sticking to the cosmological principle, the first step towards a more realistic cosmological model is to allow spatial curvature on top of ΛCDM. It is known that the Planck CMB data alone favors positive (closed space) spatial curvature, which mimics a negative energy density that varies as $\propto s^{-2}$, where s is the average expansion scale factor [4]. Moreover, spatially closed models are in agreement with not only the low CMB anisotropy quadrupole of Planck, but also the WMAP CMB data [17, 18]. However, the drastic exacerbation of the H_0 tension in this case, and the favoring of spatial flatness with extremely high precision by the Planck CMB data in combination with the baryon acoustic oscillations (BAO) data, and the astrophysical data such as type Ia Supernovae (SNIa) and cosmic chronometers (CC), have stimulated the debate on the spatial flatness assumption [4, 19–25]; particularly, given that it is in line with the canonical inflationary paradigm—yet, note that inflation is not necessarily in conflict with a non-flat space [17, 26–28], but spatially closed inflationary models are significantly fine-tuned [17]. On the other hand, the canonical inflationary paradigm—assumes a single canonical scalar field, with suitable self-interaction potential, which is minimally coupled to gravity described by GR—makes sense if the observable universe exhibits isotropic expansion (ignoring the tilted models and the possibility of being broken by, for instance, anisotropic dark energy in the late universe). Indeed, the mathematically tractable next step to generalize ΛCDM geometrically is to allow anisotropic expansion, which then leads to the generalized Friedmann equation bringing in average Hubble parameter along with the shear scalar term (quantifying the anisotropic expansion) and the spatial curvature term that deviates from $\propto s^{-2}$ behavior if the anisotropic expansion is accompanied by an anisotropic spatial curvature [29–32]. In the simplest anisotropic generalizations, viz., when the spatial curvature itself is isotropic or has negligibly small anisotropy, the spatial curvature mimics a source with a positive (open space) or negative (closed space) energy density that varies as $\propto s^{-2}$ and the shear scalar mimics a stiff fluid [33, 34] (or a canonical scalar field with a negligible potential energy compared to its kinetic energy) with a positive energy density varying as $\propto s^{-6}$, which thus dilutes faster than any other physical source (for which the stiff fluid sets the causality limit [32]) as the universe expands. The stiff fluid-like behavior of the shear scalar is typical for general relativistic anisotropic universes with isotropic spatial curvature filled only with isotropic perfect fluids with no peculiar velocities [32]. Hence, irrespective of the inflationary paradigm, it is not expected there to be an anisotropic expansion at measurable levels in the observable universe. And, given that inflation -(canonical) isotropizes the universe very efficiently, leaving almost no anisotropy even in the very early universe (cosmic no-hair theorem [35, 36]), any detection of a non-zero shear scalar today would have far reaching consequences on the standard cosmology.[1]

For instance, it is possible to generate anisotropic expansion well after decoupling, which also was suggested to address the low CMB anisotropy quadrupole [49–51], though we ignore this possibility in this work, as it demands modifications beyond pure geometry, namely, the introduction of anisotropic stresses, effective well after decoupling, from some actual sources such as vector fields or extended theories of gravity such as Brans-Dicke theory (see Refs. [42,43,52–78]). In tilted universes also, it is possible to generate/retain anisotropic expansion at late times (see footnote 1), which was suggested to address the discrepancies between the dipole amplitudes and directions from the different cosmological observations (e.g., between the radio and CMB dipoles) and even the H_0 and S_8 tensions, though we confine ourselves with orthogonal universes in this work, as tilted ones may go as far as to stop looking for corrections on top of ΛCDM and look for corrections on top of the Einstein-de Sitter universe; tilted observers (typical observers in a galaxy like the Milky Way) within the bulk flow can be misled into concluding that the universe is accelerating—it has been suggested that the indications for cosmic acceleration found in the SnIa data disappear, if a bulk flow induced anisotropy is allowed in the SnIa data, and thus, a bulk flow dipole aligned with the local bulk flow is identified while any monopole (which can be attributed to Λ) is consistent with zero [79–102] (see also Refs. [11, 12] for recent reviews and Refs. [49–51] for hints of unexpected features in CMB and other

[1]In our discussion here, we ignore the possibility of inflationary models with anisotropic hair, as it requires a departure from the canonical inflationary paradigm, which is part of the standard cosmological model intended to be investigated with its pure geometric generalization in this study. For example, non-scalar fields, in particular gauge fields, are ubiquitous in high-energy models of particle physics related to inflationary energy scales, and they can turn on in the background during inflation (or become relevant at the level of cosmic perturbations), and then lead to the violation of cosmic no-hair theorem [37–39]. And, departures from GR, e.g., quadratic curvature corrections, scalar-tensor theories of gravity such as Brans-Dicke theory with $\omega_{\rm BD} \sim -1$ (limit of the theory relevant to the string theories and d-brane constructions) can generate (or retain) anisotropic expansion [40–43]. Also, there are tilted spatially homogeneous cosmological models (with the fluid flow lines not orthogonal to the surfaces of spatial homogeneity; the components of the fluid's peculiar velocity enter as further variables) for which the tilt does not vanish at late times (once the inflation ends, anisotropic modes again occur); to an observer moving with the fluid, such models will not seem to isotropize, yet may appear isotropic in another frame at late times [44–48] (see also Refs. [31,32]).

independent cosmological data types). For such reasons, the interest in anisotropic cosmologies has never ceased and, moreover, has recently begun to rise again.

Besides these more fundamental aspects we discussed above with regard to considering the pure geometric generalization of ΛCDM by introducing spatial curvature and/or anisotropic expansion, it is tempting to explore whether these geometric generalizations by alone could be beneficial in addressing the tensions related to the ΛCDM model. Indeed, it was recently reported in Ref. [103] that the non-tilted Bianchi Type-I spacetime extension of ΛCDM, which simply allows different scale factors in three orthogonal directions on top of the spatially flat RW spacetime, relaxes the H_0 tension; it predicts $H_0 \sim 70.0$ km s^{-1} Mpc^{-1}, which agrees, within 2σ, with both the ΛCDM Planck 2018 prediction $H_0 = 67.27 \pm 0.60$ km s^{-1} Mpc^{-1} [4] and the Hubble Space Telescope (HST) and the SH0ES team local measurements, e.g., $H_0 = 73.04 \pm 1.04$ km s^{-1} Mpc^{-1} [104] (see also Refs. [105, 106]). This observation naturally makes us wondering whether the shear scalar, which is non-negative by definition, can compensate the negative energy density-like contribution of the positive (closed space) spatial curvature to the Friedmann equation, and then avoid the drastically reduced H_0 value accompanying the closed space prediction of the CMB(+Lens) data. Thus, here we will study the extension of ΛCDM allowing both non-zero spatial curvature and anisotropic expansion for mainly two reasons: (i) To test whether the latest observational data still support spatial flatness and/or isotropic expansion in this case, and, if not, (ii) to explore the roles of spatial curvature and expansion anisotropy (via its stiff fluid-like contribution to the Friedmann equation) in addressing some of the current cosmological tensions associated with the ΛCDM model.

It is also pertinent to mention that the model-independent upper bounds on the present-day expansion anisotropy in terms of its corresponding present-day density parameter ($\Omega_{\sigma 0}$) are of the order of $\mathcal{O}(10^{-3})$, e.g., from type Ia Supernovae [107–113]. This is consistent with the model-dependent constraints, $\Omega_{\sigma 0} \lesssim 10^{-3}$, obtained from the $H(z)$ and/or SNIa data (relevant to $z \lesssim 2.4$) by considering the stiff fluid-like behavior of expansion anisotropy on top of ΛCDM [103, 114]. This amount of expansion ansiotropy today, within the simplest anisotropic, i.e., the Bianchi type I spacetime, generalization of ΛCDM, implies the domination of expansion anisotropy at $z \sim 10$ and hence the spoilt of the successful description of the earlier ($z \gtrsim 10$)

universe. Indeed, the model-dependent upper bounds are usually much tighter; spanning a range from $\Omega_{\sigma 0} \lesssim 10^{-11}$ to 10^{-23} [31, 32]. When the stiff fluid-like behavior of expansion anisotropy is considered on top of ΛCDM, the constraint $\Omega_{\sigma 0} \lesssim 10^{-3}$ from the combined $H(z)$ and SnIa Pantheon data set (relevant to $z \lesssim 2.4$) is tightened to $\Omega_{\sigma 0} \lesssim 10^{-15}$ when the combined CMB+BAO data set (relevant to $z \sim 1100$) is also included, and it is further constrained to $\Omega_{\sigma 0} \lesssim 10^{-23}$ not to spoil the successes of the standard Big Bang Nucleosynthesis (BBN) (relevant to $z \sim 10^9$) [103]. We have also the typical upper bound $\Omega_{\sigma 0} \lesssim 10^{-20}$ derived from the observed CMB quadrupole temperature fluctuation $\Delta T/T \sim 10^{-5}$, which provides an upper bound at the same order of magnitude on the expansion anisotropy at the recombination era ($\sqrt{\Omega_\sigma^{\rm rec}} \sim 10^{-5}$ at $z_{\rm rec} \sim 10^3$) [115–119]. The upper bounds obtained from CMB reaches the level $\Omega_{\sigma 0} \lesssim 10^{-22}$ from the rigorous analyses of the full Planck CMB temperature and polarization data [119–121]. The BBN light element abundances also provide tight upper bounds, but at different levels depending on the presence of spatial curvature anisotropy in addition to expansion anisotropy; namely, $\Omega_{\sigma 0} \lesssim 10^{-22}$ and $\Omega_{\sigma 0} \lesssim 10^{-21}$ for the Bianchi type I and type V spacetimes (the anisotropic generalizations of the spatially flat and open RW spacetimes, respectively, and yield isotropic spatial curvature), and these relax to $\Omega_{\sigma 0} \lesssim 10^{-13}$ for the Bianchi type IX and type VII_0 spacetimes (the anisotropic generalizations of the spatially closed and open RW spacetimes, respectively, and yield anisotropic spatial curvature) [118, 122, 123].

The thesis is structured as follows: In Section 2, we describe the basic equations of the model; in Section 3, we present the data/methodology used; in Section 4, we discuss the results; and in Section 5, we summarize our findings.

2. BASIC EQUATIONS AND THE MODEL

We study a two parameter extension of the ΛCDM model that allows both non-zero spatial curvature and anisotropic expansion, both which are geometric corrections on top of the base ΛCDM model. The fundamental idea here is to extend ΛCDM just by relaxing its spatially flat RW metric assumption to a more realistic one. Accordingly, we consider the generalized Friedmann equation which, compared to the usual one, includes two new parameters, viz., the spatial curvature (pertaining to deviation from flat space) and the shear scalar (pertaining to deviation from isotropic expansion);

$$3H^2 + \frac{1}{2}\,{}^3R - \sigma^2 = 8\pi G\rho, \tag{2.1}$$

where H is the average Hubble parameter defined as $H \equiv \frac{1}{3}\Theta$ ($\Theta = \mathrm{D}^\mu u_\mu$ is the volume expansion rate with D^μ being the fully orthogonally projected covariant derivative and u_μ is the four-velocity that satisfies $u_\mu u^\mu = -1$ and $\nabla_\nu u^\mu u_\mu = 0$), ${}^3R$ is the 3-Ricci scalar (the Ricci scalar of the spatial section of the spacetime metric), σ^2 is the shear scalar quantifying the anisotropic expansion ($\sigma^2 = \frac{1}{2}\sigma_{\alpha\beta}\sigma^{\alpha\beta}$, where $\sigma_{\alpha\beta} = \frac{1}{2}(u_{\mu;\nu} + u_{\nu;\mu})h^\mu_\alpha h^\nu_\beta - \frac{1}{3}u^\mu_{;\mu}h_{\alpha\beta}$ is the shear tensor with $h_{\mu\nu} = g_{\mu\nu} + u_\mu u_\nu$ being the projection tensor into the instantaneous rest frame of comoving observers), G is the Newton's gravitational constant, and ρ is the energy density of the total physical ingredient of the universe (see Refs. [29–32]). In this work, we limit our investigations to the orthogonal (non-tilted) models—the fluid flow lines are orthogonal to the surfaces of spatial homogeneity—, as the tilted ones—the fluid flow lines are not orthogonal to the surfaces of spatial homogeneity—are significantly more complicated and bringing in the components of the fluid's peculiar velocity as additional variables on top of the the fluid's energy density and pressure; the spatial curvature and shear scalar already introduce two new free parameters to be constrained on top of the ΛCDM model (see Refs. [31, 32]).

We use the Einstein field equations (EFE) of GR;

$$G_{\mu\nu} \equiv R_{\mu\nu} - \frac{1}{2}g_{\mu\nu}R = 8\pi G T_{\mu\nu}, \tag{2.2}$$

where $G_{\mu\nu}$ is the Einstein tensor, $R_{\mu\nu}$ is the Ricci tensor, R is the Ricci scalar, and $g_{\mu\nu}$ is the metric tensor. We suppose all types of matter distributions (viz., the usual cosmological sources such as radiation, baryons, etc.) are perfect fluids with no peculiar velocities, described by the energy-momentum tensor (EMT) of the form $T_{\mu}^{\nu} = \mathrm{diag}[-\rho, p, p, p]$, where ρ and p are the energy density and pressure, respectively. EFE (2.2) satisfy $T^{\mu\nu}{}_{;\nu} = 0$ (the conservation equation for the total EMT representing all sources in the universe) via $G^{\mu\nu}{}_{;\nu} = 0$ as a consequence of the twice-contracted Bianchi identity. This leads to the continuity equation for the total EMT: $\dot{\rho} + 3H(\rho + p) = 0$, where the dot represents the derivative with respect to the proper time t. We consider the usual cosmological sources, namely, pressureless fluid (CDM, baryons) described by the equation of state (EoS) $p_{\mathrm{m}}/\rho_{\mathrm{m}} = 0$, radiation (photons γ, neutrinos ν) described by the EoS $p_{\mathrm{r}}/\rho_{\mathrm{r}} = \frac{1}{3}$, and DE mimicked by a cosmological constant (viz., $\rho_{\Lambda} = \frac{\Lambda}{8\pi G} = \mathrm{const}$) described by the EoS $p_{\Lambda}/\rho_{\Lambda} = -1$. We suppose these sources interact only gravitationally, so that the continuity equation is satisfied separately by each source, and this leads to

$$\rho \equiv \rho_{\mathrm{r}} + \rho_{\mathrm{m}} + \rho_{\Lambda} = \rho_{\mathrm{r}0} s^{-4} + \rho_{\mathrm{m}0} s^{-3} + \rho_{\Lambda} \tag{2.3}$$

where $s \equiv v^{1/3}$ is the mean scale factor with v being the volume scale factor. The present-day value of s is set as $s_0 = 1$. Here and onward, a subscript 0 attached to any quantity implies its value in the present-day universe. Note that the present-day photon energy density $\rho_{\mathrm{r}0}$ is extremely well constrained by the absolute CMB monopole temperature measured by FIRAS $T_0 = 2.7255 \pm 0.0006\,\mathrm{K}$ [124], and thereby its present-day density parameter given by $\Omega_{\mathrm{r}0} \equiv \rho_{\mathrm{r}0}/3H_0^2 = 2.469 \times 10^{-5} h^{-2}(1 + 0.2271 N_{\mathrm{eff}})$—where $h = H_0/100\,\mathrm{km\,s^{-1}Mpc^{-1}}$ is the dimensionless reduced Hubble constant and $N_{\mathrm{eff}} = 3.046$ is the standard number of effective neutrino species with minimum allowed mass $m_{\nu} = 0.06$ eV—is not subject to our observational analysis.

To fully determine the modified Friedmann equation (2.1), viz., $H(s)$, however, it is necessary to determine the evolution of the two remaining parameters, namely, the functions ${}^{3}R(s)$ and $\sigma^2(s)$. In what follows, we first present explicit constructions of different cases extending ΛCDM and then write a single $H(s)$ function including all these cases to be constrained with the observational data. To do so, we start with the spatially maximally symmetric metric, the RW metric, for the purpose of comparison with the three spatially homogeneous but not necessarily isotropic metrics, namely, the Bianchi type I, Bianchi type V, and Bianchi type IX metrics which are the simplest anisotropic generalizations of the spatially flat, open, and closed RW metrics, respectively.

2.1 Spatially Homogeneous And Isotropic Universe

We start with the RW metric; respecting the cosmological principle, it yields maximally symmetric spatial section (not necessarily flat), and it can be written in Cartesian coordinates as follows:

$$\mathrm{d}s^2 = -\mathrm{d}t^2 + s^2 \frac{\mathrm{d}x^2 + \mathrm{d}y^2 + \mathrm{d}z^2}{\left[1 + \frac{\kappa}{4}(x^2 + y^2 + z^2)\right]^2}, \tag{2.4}$$

where $\kappa < 0$, $\kappa = 0$, and $\kappa > 0$ correspond to spatially open, flat, and closed universes, respectively. EFE in (2.2) for the RW metric in (2.4) lead to the following set of differential equations, viz., the usual Friedmann equations;

$$3\frac{\dot{s}^2}{s^2} + 3\frac{\kappa}{s^2} = 8\pi G\rho, \tag{2.5}$$

$$-2\frac{\ddot{s}}{s} - \frac{\dot{s}^2}{s^2} - \frac{\kappa}{s^2} = 8\pi G p. \tag{2.6}$$

The shear scalar and 3-Ricci scalar for the RW metric in (2.4) read

$$\sigma^2 = 0 \quad \text{and} \quad {}^3R = {}^3R_0 s^{-2}, \tag{2.7}$$

where ${}^3R_0 = 6\kappa$.

In what follows, we will refer this well known generalization of the standard ΛCDM model, which simply allows non-zero spatial curvature on top it, to as the $o\Lambda$CDM model, where "o" stands for "spatial curvature".

2.2 Spatially Homogeneous, Flat And Anisotropic Universe

We continue with the Bianchi type I metric, which simply allows different scale factors in three orthogonal directions on top of the spatially flat ($\kappa = 0$) RW metric, while preserving isotropic spatial curvature;

$$\mathrm{d}s^2 = -\mathrm{d}t^2 + a^2\mathrm{d}x^2 + b^2\mathrm{d}y^2 + c^2\mathrm{d}z^2, \tag{2.8}$$

where $\{a, b, c\} = \{a(t), b(t), c(t)\}$ are the directional scale factors along the principal axes $\{x, y, z\}$ and are functions of t only. The corresponding average expansion scale factor is $s = (abc)^{\frac{1}{3}}$ and from which the average Hubble parameter is defined as $H = \frac{\dot{s}}{s} = \frac{1}{3}(H_x + H_y + H_z)$, where $H_x = \frac{\dot{a}}{a}$, $H_y = \frac{\dot{b}}{b}$ and $H_z = \frac{\dot{c}}{c}$ are the directional Hubble parameters defined along the x-, y-, and z-axes, respectively.

EFE in (2.2) for the Bianchi type I metric in (2.8) lead to the following set of differential equations:

$$\frac{\dot{a}}{a}\frac{\dot{b}}{b} + \frac{\dot{b}}{b}\frac{\dot{c}}{c} + \frac{\dot{a}}{a}\frac{\dot{c}}{c} = 8\pi G\rho, \tag{2.9}$$

$$-\frac{\ddot{b}}{b} - \frac{\ddot{c}}{c} - \frac{\dot{b}}{b}\frac{\dot{c}}{c} = 8\pi G p, \tag{2.10}$$

$$-\frac{\ddot{a}}{a} - \frac{\ddot{c}}{c} - \frac{\dot{a}}{a}\frac{\dot{c}}{c} = 8\pi G p, \tag{2.11}$$

$$-\frac{\ddot{a}}{a} - \frac{\ddot{b}}{b} - \frac{\dot{a}}{a}\frac{\dot{b}}{b} = 8\pi G p. \tag{2.12}$$

The shear scalar, in terms of the directional Hubble parameters, reads

$$\sigma^2 = \frac{(H_x - H_y)^2 + (H_y - H_z)^2 + (H_z - H_x)^2}{6}. \tag{2.13}$$

We can rewrite equations (2.10)-(2.12) as follows;

$$\dot{H}_x - \dot{H}_y + 3H(H_x - H_y) = 0, \tag{2.14}$$

$$\dot{H}_y - \dot{H}_z + 3H(H_y - H_z) = 0, \tag{2.15}$$

$$\dot{H}_z - \dot{H}_x + 3H(H_z - H_x) = 0, \tag{2.16}$$

and then, using these along with the time derivative of σ^2 given in equation (2.13), we reach the shear propagation equation

$$\dot{\sigma} + 3H\sigma = 0. \tag{2.17}$$

Its integration yields

$$\sigma^2 = \sigma_0^2 s^{-6}. \tag{2.18}$$

The 3-Ricci scalar for the Bianchi type I metric in (2.8) is null;

$${}^3R = 0, \tag{2.19}$$

which corresponds to a flat space, likewise the spatially flat ($\kappa = 0$) RW metric.

In what follows, we refer to the Bianchi type I extension of the standard ΛCDM model as An-ΛCDM model, where "An" stands for "anisotropic".

2.3 Spatially Homogeneous, Open And Anisotropic Universe

We next continue with the Bianchi type V metric, which simply allows different scale factors in three orthogonal directions on top of the spatially open ($\kappa < 0$) RW metric, while preserving isotropic spatial curvature;

$$\mathrm{d}s^2 = -\mathrm{d}t^2 + a^2 e^{-2mz}\mathrm{d}x^2 + b^2 e^{-2mz}\mathrm{d}y^2 + c^2\mathrm{d}z^2, \tag{2.20}$$

where $m \neq 0$ is a non-zero real constant. It can be observed that Bianchi type V metric in (2.20) reduces to the Bianchi type I metric in (2.8) when $m = 0$.

EFE in (2.2) for the Bianchi type V metric in (2.20) lead to the following set of differential equations:

$$\frac{\dot{a}}{a}\frac{\dot{b}}{b} + \frac{\dot{a}}{a}\frac{\dot{c}}{c} + \frac{\dot{b}}{b}\frac{\dot{c}}{c} - 3\frac{m^2}{c^2} = 8\pi G\rho, \tag{2.21}$$

$$-\frac{\ddot{b}}{b} - \frac{\ddot{c}}{c} - \frac{\dot{b}}{b}\frac{\dot{c}}{c} + \frac{m^2}{c^2} = 8\pi G p, \tag{2.22}$$

$$-\frac{\ddot{a}}{a} - \frac{\ddot{c}}{c} - \frac{\dot{a}}{a}\frac{\dot{c}}{c} + \frac{m^2}{c^2} = 8\pi G p, \tag{2.23}$$

$$-\frac{\ddot{a}}{a} - \frac{\ddot{b}}{b} - \frac{\dot{a}}{a}\frac{\dot{b}}{b} + \frac{m^2}{c^2} = 8\pi G p, \tag{2.24}$$

$$m\left(2\frac{\dot{c}}{c} - \frac{\dot{a}}{a} - \frac{\dot{b}}{b}\right) = 0. \tag{2.25}$$

In equation (2.25), we see the component $G^0{}_3 = 8\pi G T^0_3$, where we take $T^0_3 = 0$ as we consider only perfect fluid distributions; i.e., T^{0i} the energy flux density (which equals the momentum density T^{i0}) is not allowed. As a result of this, solving equation (2.25), it turns out that

$$c = c_1 (ab)^{\frac{1}{2}}, \tag{2.26}$$

where $c_1 > 0$ is the integration constant. As we set $s_0 = 1$, the present-day values of the directional scale factors, i.e., $a_0 > 0$, $b_0 > 0$, and $c_0 > 0$, must satisfy $a_0 b_0 c_0 = 1$, and therefore $c_1 = (a_0 b_0)^{-\frac{3}{2}}$. Accordingly, we re-express the average expansion scale factor as $s = (a_0 b_0)^{-\frac{1}{2}}(ab)^{\frac{1}{2}}$, which in turn implies $c = a_0 b_0 s$. Using equation (2.26), the set of field equations (2.21)-(2.24) reduces to

$$2\frac{\dot{a}}{a}\frac{\dot{b}}{b}+\frac{1}{2}\frac{\dot{a}^2}{a^2}+\frac{1}{2}\frac{\dot{b}^2}{b^2}-3\frac{m^2}{ab}=8\pi G\rho, \tag{2.27}$$

$$-\frac{3}{2}\frac{\ddot{b}}{b}-\frac{1}{2}\frac{\ddot{a}}{a}+\frac{1}{4}\frac{\dot{a}^2}{a^2}-\frac{1}{4}\frac{\dot{b}^2}{b^2}-\frac{\dot{a}}{a}\frac{\dot{b}}{b}+\frac{m^2}{ab}=8\pi Gp, \tag{2.28}$$

$$-\frac{3}{2}\frac{\ddot{a}}{a}-\frac{1}{2}\frac{\ddot{b}}{b}-\frac{1}{4}\frac{\dot{a}^2}{a^2}+\frac{1}{4}\frac{\dot{b}^2}{b^2}-\frac{\dot{a}}{a}\frac{\dot{b}}{b}+\frac{m^2}{ab}=8\pi Gp, \tag{2.29}$$

$$-\frac{\ddot{a}}{a}-\frac{\ddot{b}}{b}-\frac{\dot{a}}{a}\frac{\dot{b}}{b}+\frac{m^2}{ab}=8\pi Gp. \tag{2.30}$$

Also, the average Hubble parameter reduces to

$$H=\frac{1}{2}(H_x+H_y), \tag{2.31}$$

and the shear scalar in (2.13) reduces to

$$\sigma^2=\frac{1}{4}(H_x-H_y)^2. \tag{2.32}$$

Subtracting equation (2.30) from equation (2.28) [or equation (2.29)] we obtain

$$2\frac{\ddot{a}}{a}-2\frac{\ddot{b}}{b}+\frac{\dot{a}^2}{a^2}-\frac{\dot{b}^2}{b^2}=0, \tag{2.33}$$

which, after using H in (2.31) and σ^2 in (2.32), leads to the shear propagation equation in the form

$$\dot{\sigma}+3H\sigma=0. \tag{2.34}$$

From its integration, we obtain

$$\sigma^2=\sigma_0^2 s^{-6}, \tag{2.35}$$

as in the case of the Bianchi type I metric, see equation (2.18). The 3-Ricci scalar for the Bianchi type V metric in (2.20) reads

$${}^3R={}^3R_0 s^{-2}, \tag{2.36}$$

which is negative definite, as here ${}^3R_0=-6c_0m^2<0$, corresponding to an open space; e.g., to compare with the spatially open ($\kappa<0$) RW metric, when we set $a=b=c$ (so that $a_0=b_0=c_0=1$ as $s_0=1$), we find $-m^2=\kappa<0$.

Note that the non-zero components of the 3-Ricci tensors for the Bianchi type V metric are as follows:

$${}^3R^1_1={}^3R^2_2={}^3R^2_2=-\frac{2m^2}{c^2}, \tag{2.37}$$

It can be observed that 3-Ricci tensors are all identical meaning that the metric has an isotropic spatial curvature.

2.4 Spatially Homogeneous, Closed And Anisotropic Spacetime

Finally, we consider the Bianchi type IX metric, which allows a different scale factor along only one [as, for simplicity sake, we consider the locally rotationally symmetric (LRS) case] of the principal axes on top the spatially closed RW metric, described by

$$\begin{aligned} \mathrm{d}s^2 = &-\mathrm{d}t^2 + a^2\mathrm{d}x^2 + b^2\mathrm{d}y^2 \\ &+ \left(b^2\sin^2 2ny + a^2\cos^2 2ny\right)\mathrm{d}z^2 - 2a^2\cos 2ny\,\mathrm{d}x\mathrm{d}z, \end{aligned} \tag{2.38}$$

where $n \neq 0$ is a non-zero real constant. It reduces to the LRS Bianchi type I metric (i.e., the Bianchi type I metric in (2.8) with $c = b$, leading to $H_z = H_y$) for $n = 0$. We note that, unlike the Bianchi type I and type V metrics, this metric yields anisotropic spatial curvature, which would alter the evolution $\sigma^2 \propto s^{-6}$ of the shear scalar. The corresponding average expansion scale factor and average Hubble parameter respectively read as $s = (ab^2)^{\frac{1}{3}}$ and $H = \frac{1}{3}(H_x + 2H_y)$.

EFE in (2.2) for the Bianchi type IX metric in (2.38) lead to the following set of differential equations:

$$2\frac{\dot{a}}{a}\frac{\dot{b}}{b} + \frac{\dot{b}^2}{b^2} + n^2\left(\frac{4}{b^2} - \frac{a^2}{b^4}\right) = 8\pi G\rho, \tag{2.39}$$

$$-2\frac{\ddot{b}}{b} - \frac{\dot{b}^2}{b^2} - n^2\left(\frac{4}{b^2} - 3\frac{a^2}{b^4}\right) = 8\pi G p, \tag{2.40}$$

$$-\frac{\ddot{a}}{a} - \frac{\ddot{b}}{b} - \frac{\dot{a}}{a}\frac{\dot{b}}{b} - n^2\frac{a^2}{b^4} = 8\pi G p. \tag{2.41}$$

The shear scalar, in terms of the directional Hubble parameters, reads

$$\sigma^2 = \frac{1}{3}(H_x - H_y)^2. \tag{2.42}$$

Subtracting equation (2.41) from equation (2.40), we obtain

$$\frac{\ddot{b}}{b} + \frac{\dot{b}^2}{b^2} - \frac{\ddot{a}}{a} - \frac{\dot{a}}{a}\frac{\dot{b}}{b} + 4n^2\left(\frac{1}{b^2} - \frac{a^2}{b^4}\right) = 0. \tag{2.43}$$

Rewriting the first four terms here in terms of H and σ^2 given in equation (2.42), we obtain the shear propagation equation as follows:

$$\dot{\sigma} + 3H\sigma = \frac{4n^2}{\sqrt{3}}\left(\frac{1}{b^2} - \frac{a^2}{b^4}\right). \tag{2.44}$$

The 3-Ricci scalar for the Bianchi type IX metric in (2.38) reads

$$^3R = 2n^2\left(\frac{4}{b^2} - \frac{a^2}{b^4}\right), \tag{2.45}$$

with the present day value, ${}^3R_0 = 2n^2\left(\frac{4}{b_0^2} - \frac{a_0^2}{b_0^4}\right)$.

Note that the non-zero components of the 3-Ricci tensors for the Bianchi type IX metric are as follows:

$$ {}^3R^1_1 = 2n^2\frac{a^2}{b^4}, \quad \text{and} \quad {}^3R^2_2 = {}^3R^3_3 = 2n^2\left(\frac{2}{b^2} - \frac{a^2}{b^4}\right). \tag{2.46} $$

It can be observed that 3-Ricci tensors are not all identical which means that the metric has an anisotropic spatial curvature.

To solve shear propagation equation (2.44) we need to obtain scale factors a and b in terms of σ^2 and H. Using the definition of H we can rewrite H_x in terms of H_y as

$$ H_x = 3H - 2H_y. \tag{2.47} $$

Substituting equation (2.47) into equation (2.42) we get

$$ \sigma = \sqrt{3}(H - H_y). \tag{2.48} $$

From equation (2.48) H_y yields to

$$ \frac{\dot{b}}{b} = H - \frac{\sigma}{\sqrt{3}}. \tag{2.49} $$

Integrating equation (2.49) and using s we obtain the scale factor b along the y- axis and scale factor a along the x- axis in terms of H and σ^2 as follows

$$ a = a_0 s^3 e^{-2\int(H - \frac{1}{\sqrt{3}\sigma})\mathrm{d}t}, \tag{2.50} $$

$$ b = b_0 e^{\int(H - \frac{1}{\sqrt{3}\sigma})\mathrm{d}t}. \tag{2.51} $$

Hence, $H = \frac{\dot{s}}{s}$ in equations (2.50) and (2.51) reduce to the following form

$$ a = a_0 s e^{2\int \frac{1}{\sqrt{3}\sigma}\mathrm{d}t}, \tag{2.52} $$

$$ b = b_0 s e^{-\int \frac{1}{\sqrt{3}\sigma}\mathrm{d}t}. \tag{2.53} $$

Using $\mathrm{d}t = -\frac{dz}{H(1+z)}$ where z is the cosmic redshift we define in terms of s as $z = -1 + \frac{1}{s}$, we re-express equations (2.54) and (2.53) as

$$ a = a_0(1+z)^{-1} e^{-2\int \frac{\sigma}{\sqrt{3}H(1+z)}\mathrm{d}z}, \tag{2.54} $$

$$ b = a_0^{-\frac{1}{2}}(1+z)^{-1} e^{\int \frac{\sigma}{\sqrt{3}H(1+z)}\mathrm{d}z}. \tag{2.55} $$

As we set $s_0 = s(z=0) = 1$, a_0 and b_0 must satisfy $a_0 b_0^2 = 1$, and therefore we used $b_0 = a_0^{-\frac{1}{2}}$. Substituting equations (2.50) and (2.51) into equation (2.44) we obtain shear propagation equation only in terms of σ^2 and s as

$$\dot{\sigma} + 3\frac{\dot{s}}{s}\sigma = \frac{1}{\sqrt{3}} n^2 \left(b_0^{-2} s^{-2} e^{2\int \frac{\sigma}{\sqrt{3}}\mathrm{d}t} - \frac{a_0^2}{b_0^4} s^{-2} \right). \tag{2.56}$$

Equation (2.56) can be rewritten as a function of the cosmic redshift z as

$$\frac{\mathrm{d}\sigma}{\mathrm{d}z} - \frac{3\sigma}{1+z} = \frac{1+z}{\sqrt{3}H} n^2 \left(1 - a_0 e^{-2\int \frac{\sigma}{\sqrt{3}H(1+z)}\mathrm{d}z} \right). \tag{2.57}$$

Integration of equation (2.57) gives the contribution of the expansion anisotropy as a function of z however we could not obtain analytically an exact cosmological solution of equation (2.57). Hence, we now suppose that the Universe, all the way to the recombination, exhibits similar expansion histories along all the principal axes, i.e.,

$$a \simeq b \simeq s, \tag{2.58}$$

so that $a_0 \simeq b_0 \simeq s_0$, satisfying $s_0^3 = a_0 b_0^2 = 1$. This is in line with the observed CMB quadrupole temperature fluctuation ($\Delta T/T \sim 10^{-5}$) setting an upper limit at the same order of magnitude on the expansion anisotropy at the recombination era ($\sqrt{\Omega_\sigma^{\mathrm{rec}}} \sim 10^{-5}$ at $z_{\mathrm{rec}} \sim 10^3$), which transforms to the typical upper limit $\Omega_{\sigma 0} \sim 10^{-20}$ derived from $\sigma^2 \propto s^{-6}$ relation [115–119]. Accordingly, the shear propagation equation (2.44) can approximately be written as follows:

$$\dot{\sigma} + 3H\sigma \simeq 0, \tag{2.59}$$

from which the shear scalar approximately reads

$$\sigma^2 \simeq \sigma_0^2 s^{-6}. \tag{2.60}$$

Similarly, the 3-Ricci scalar equation (2.45) can approximately be written as follows:

$${}^3R \simeq {}^3R_0 s^{-2}, \tag{2.61}$$

which is positive definite, as here ${}^3R_0 \simeq 6n^2 > 0$, corresponding to a closed space; e.g., to compare with the spatially closed ($\kappa > 0$) RW metric, when we set $a = b = s$ (so that $a_0 = b_0 = 1$ as $s_0 = 1$) we find $n^2 = \kappa > 0$. Thus, in the case, for small anisotropies, the modified Friedmann equation (2.1) can approximately be written by using $\sigma^2 = \sigma_0^2 s^{-6}$, likewise in the cases of the Bianchi type I and type V metrics, and ${}^3R = {}^3R_0 s^{-2} > 0$, likewise in the case of the spatially closed ($\kappa > 0$) RW metric.

2.5 Spatially Homogeneous, But Not Necessarily Flat And Isotropic, Spacetime Extension Of The ΛCDM Model

The generalized Friedmann equation for the spatially homogeneous, but not necessarily flat and isotropic, spacetime metric and the non-tilted perfect fluids that we will confront with the observational data, can be written as follows:

$$3H^2 = 8\pi G(\rho + \rho_\kappa + \rho_\sigma), \tag{2.62}$$

where ρ is the energy density of the total physical ingredient of the universe given in equation (2.3), while ρ_κ and ρ_σ are the effective energy densities corresponding to spatial curvature (viz., the 3-Ricci scalar) and expansion anisotropy (viz., the shear scalar) through the following definitions, correspondingly,

$$\rho_\kappa = \frac{-\frac{1}{2}\,{}^3R}{8\pi G} \quad \text{and} \quad \rho_\sigma = \frac{\sigma^2}{8\pi G}. \tag{2.63}$$

Consequently, using ρ from equation (2.3) along with the 3-Ricci scalars and the shear scalars obtained above, we reach the following single generalized Friedmann equation, describing the spatially homogeneous, but not necessarily flat and isotropic, and non-tilted extension of the ΛCDM model, to be confronted with the observational data:

$$\frac{H^2(s)}{H_0^2} = \Omega_{\sigma 0}s^{-6} + \Omega_{\mathrm{r}0}s^{-4} + \Omega_{\mathrm{m}0}s^{-3} + \Omega_{\kappa 0}s^{-2} + \Omega_{\Lambda 0}, \tag{2.64}$$

where the present-day density parameters satisfy $\Omega_{\sigma 0} + \Omega_{\mathrm{r}0} + \Omega_{\mathrm{m}0} + \Omega_{\kappa 0} + \Omega_{\Lambda 0} = 1$ and among which $\Omega_{\kappa 0}$ and $\Omega_{\sigma 0}$ are geometric terms; namely, $\Omega_{\kappa 0}$ stands for the spatial curvature, which can be $\Omega_{\kappa 0} = 0$, $\Omega_{\kappa 0} > 0$, and $\Omega_{\kappa 0} < 0$, corresponding to the spatially flat, open, and closed universes, respectively, and $\Omega_{\sigma 0} \geq 0$ stands for expansion anisotropy (viz., the shear scalar), which is non-negative definite.

In what follows, we call this model, described by equation (2.64), An-$o\Lambda$CDM model. We note that the An-$o\Lambda$CDM model is mathematically equivalent to adding stiff/Zeldovich fluid [33, 34] on top of the $o\Lambda$CDM model, though these two models are physically different. Namely, the new term $\Omega_{\sigma 0}s^{-6}$ on top of the $o\Lambda$CDM model contributes to the Friedmann equation like a source called stiff fluid described by the EoS of the form $p_{\mathrm{s}}/\rho_{\mathrm{s}} = 1$, but in the An-$o\Lambda$CDM model, this term arises from the anisotropic expansion.

In other words, here, $H(s)$ is the average expansion rate and the expansion rates along the different principal axes need not necessarily be the same. Yet, we can define an average redshift as $z=-1+\frac{1}{s}$ from the average expansion scale factor s, and then rewrite this equation in terms of z for observational analysis purposes at the background level. The observational analysis relying on this approach will then reflect *only* the stiff fluid-like effect of the expansion anisotropy on the average expansion rate, $H(s)$, of the An-$o\Lambda$CDM model. This in turn implies that the constraints, that we will obtain in this work, can be adopted for the cosmological models that contain a stiff "fluid" on top of the ΛCDM and $o\Lambda$CDM models.[1]

For the observational analysis of the models, we will use SNIa and cosmic chronometers (CC) data relevant to the late universe (viz., $z \lesssim 2.4$), and BAO and CMB data relevant to the universe since the recombination (viz., the drag redshift $z_{\rm d} \sim 1060$ and last scattering redshift $z_* \sim 1090$ involved in BAO and CMB data analyses, respectively). In order to quantify the amount/effects of expansion anisotropy within the framework of the considered theoretical model described by equation (2.64) using the observational data, we have two main options: (i) We can perform a full likelihood treatment of the data, so that, for instance, using the late time observational data, which incorporates the location of objects (e.g., SNIa) in the sky, and can in principle be able to distinguish between anisotropic expansion and stiff fluid. (ii) We may explore the observational constraints on the model at the background level. We prefer to proceed with the second approach for the reasons explained in detail below.

A full likelihood treatment of the late time observational data, which incorporates the location of objects (e.g., SNIa) in the sky, can in principle be able to distinguish between anisotropic expansion and stiff fluid, as these likelihoods use the differing z and $H(z)$ values along different axes of line of sight and incorporate these in an object-by-object differentiation of the cosmological distances entering the likelihoods. Such an approach would inevitably be necessary, e.g., in tilted models, since in this case determining the dipole amplitudes and directions from different cosmological

[1]Cosmologies with a stiff fluid era stemming from different underpinning theories are ubiquitous, but differ in details (in particular, their perturbations and hence their imprints on the CMB anisotropies are different [125, 126]), see Ref. [127] for a general discussion (theoretical) on the ΛCDM+stiff fluid cosmology, and Refs. [33,34,61,128–131,131–145] for some particular models of this type that include sources (actual or effective) that resemble stiff fluid (permanently or temporarily).

observations would have far-reaching consequences that may be beyond seeking corrections on top of ΛCDM, as discussed also in the introduction (Sec. 1). However, in our case, assuming non-tilted perfect fluids as in the standard cosmological model, this would work most efficiently if the shear scalar was not predicted to resemble a stiff fluid ($\sigma^2 \propto s^{-6}$) by GR, but a source that exhibits a much flatter average expansion scale factor dependence. For example, suppose the shear scalar resembles dust ($\sigma^2 \propto s^{-3}$) via an anisotropic dark energy or a modified theory of gravity (see Refs. [42, 43, 52–78]). In this case, unless a full likelihood treatment of the observational data is performed, the constraints on the present-day density parameters of a dust-like shear scalar and actual dust components would degenerate. On the other hand, in the case anisotropic expansion is allowed on top of ΛCDM or *o*ΛCDM, the stiff fluid approach is not less robust in determining constraints on the $\Omega_{\sigma 0}$ parameter, although it cannot map the state of expansion anisotropy in the sky. In particular, when using the data relevant to relatively late universe (e.g., SNIa), the model independent constraints—which naturally consider full likelihoods—on $\Omega_{\sigma 0}$ and the ones from the stiff fluid like behaviour of the shear scalar only provide us with upper bounds, and these are at almost the same order of magnitude in the two different approaches, viz., $\Omega_{\sigma 0} \lesssim 10^{-3}$ [103, 107–114]. Also, in the stiff fluid approach on top of ΛCDM, the upper bounds obtained by using the compressed BAO and/or CMB data are already much stronger, $\Omega_{\sigma 0} \lesssim 10^{-15}$; leaving anisotropic expansion on top of ΛCDM only as a correction (see [103] and references therein), at least all the way the recombination. That is, even if the compressed BAO and/or CMB data are used instead of full data, it does not matter for the determination of $\Omega_{\sigma 0}$ whether the full likelihoods of the data relevant to late universe (e.g., SNIa, CC) are used or not.

It is also worth noting that introducing isotropic (or almost isotropic) spatial curvature, viz., the $\Omega_{\kappa 0} s^{-2}$ term, on top of ΛCDM is similar to introducing a source described by the EoS of the form $p_{\rm cs}/\rho_{\rm cs} = -1/3$, such as cosmic strings (which can also have negative mass density [146]). Accordingly, the An-*o*ΛCDM model, the pure geometric generalization of ΛCDM discussed here, resembles a cosmological model with cosmic strings (CS) and a stiff fluid with a positive energy density on top of ΛCDM. However, strictly speaking, this should only be considered true at the background level; a spatial curvature term in the background and a source with $w = -1/3$, and similarly, the shear scalar term and a source with $w = 1$, give identical contributions to $H(s)$, the volumetric expansion rate of the Universe, but are not similar in their contribution to CMB anisotropies [125, 126, 147]. Not to mention that the perturbations, hence the CMB anisotropies, will differ when anisotropic expansion is allowed on top of the RW spacetime, moreover they also differ depending on the theoretical models (see footnote 1) that introduce a stiff fluid like contribution on top of ΛCDM [125, 126, 147].

For these reasons, exploring the observational constraints on An-$o\Lambda$CDM at the background level would provide us the opportunity to interpret these results also as constraints on a large family of cosmological models containing stiff fluid on top of ΛCDM and $o\Lambda$CDM, rather than a particular model (each of which may be a separate research topic); compromising the details of the underpinning physics/theoretical model (see footnote 1) giving rise to stiff fluid type contributions in the Friedmann equation. These models can, of course, be further constrained when, for instance, the full CMB data are used and they can then be distinguished from each other based on their perturbation differences. Lastly, the strongest upper bounds on anisotropic expansion are obtained from the CMB quadrupole ($l = 2$ corresponds to the angular scale $\theta = \pi/2$ on the sky) temperature fluctuation ($\Delta T_{\rm Planck} \approx 10\,\mu$K [148], relevant to perturbations) and/or BBN, viz., $\Omega_{\sigma 0} \lesssim 10^{-21} - 10^{-23}$ (see [103] and references therein). Compromising these in our analysis, implying relatively weaker constraints, may be seen as a drawback, but this is preferred on purpose in the current work; in this case, we would be able to assess whether the presence of anisotropy, as a correction, yet at a level beyond the one imposed by the full CMB and/or BBN data, on top of ΛCDM and $o\Lambda$CDM could have consequences on the H_0 tension [9] and/or the spatial curvature ($\Omega_{\kappa 0}$) tension [8], which, in fact, is the main motivation of the current work, rather than finding new improved constraints on the expansion anisotropy and spatial curvature, when introduced on top of the standard cosmological model.

3. DATA AND LIKELIHOODS

In this section, we briefly describe the used data sets, and the adopted methodology to perform the observational analyses.

3.1 Cosmic Chronometers

We consider the compilation of 31 cosmic chronometer (CC) measurements of $H(z)$ lying in the redshift range $0.07 \leq z \leq 1.965$, as shown in Table I of [24], and the references therein. The principle, underlying these measurements, was first proposed in [149], relating the Hubble parameter $H(z)$, redshift z, and cosmic time t as

$$H(z) = -\frac{1}{1+z}\frac{\mathrm{d}z}{\mathrm{d}t}. \tag{3.1}$$

The chi-squared function for these measurements, denoted by χ^2_{CC}, is

$$\chi^2_{\mathrm{CC}} = \sum_{i=1}^{31} \frac{[H^{\mathrm{obs}}(z_i) - H^{\mathrm{th}}(z_i)]^2}{\sigma^2_{H^{\mathrm{obs}}(z_i)}}, \tag{3.2}$$

where $H^{\mathrm{obs}}(z_i)$ is the observed value of the Hubble parameter with the standard deviation $\sigma^2_{H^{\mathrm{obs}}(z_i)}$ as given in the aforementioned table, and $H^{\mathrm{th}}(z_i)$ is the theoretical value obtained from the cosmological model under consideration.

3.2 SnIa (Pantheon 2018)

The Pantheon 2018 (Pan) sample comprises a large type Ia supernovae sample of 1048 measurements from five subsamples PS1, SDSS, SNLS, low-z, and HST spanning in the redshift range $0.01 < z < 2.3$ [103, 150, 151].

The chi-squared function of the Pan data is given by

$$\chi^2_{\mathrm{Pan}} = \Delta\mu\, C^{-1}_{\mathrm{Pan}}\, \Delta\mu^T\,, \tag{3.3}$$

where $\Delta\mu = \mu_i^{\mathrm{obs}} - \mu^{\mathrm{th}}$. The observed distance modulus (μ_i^{obs}) [152] is evaluated as

$$\mu_i^{\mathrm{obs}} = \mu_{B,i} + \mathcal{M}, \tag{3.4}$$

where $\mu_{B,i}$ is the observed peak magnitude at maximum in the rest frame of the B band for redshift z_i, while the quantity $\mathcal{M}$ is the nuisance parameter. On the other hand, we evaluate the theoretical distance modulus as

$$\mu^{\rm th} = 5\log_{10} D_L + \mathcal{M}, \tag{3.5}$$

where

$$D_L = (1+z_{\rm hel}) \int_0^{z_{\rm cmb}} \frac{H_0 dz}{H(z)}, \tag{3.6}$$

with $z_{\rm hel}$ and $z_{\rm cmb}$ being the heliocentric and CMB rest frame redshifts, respectively.

The covariance matrix is measured as [153],

$$C_{\rm Pan} = C_{\rm sys} + D_{\rm stat}, \tag{3.7}$$

where $C_{\rm sys}$ is the systematic covariance matrix. Further, $D_{\rm stat}$ is the diagonal covariance matrix of the statistical uncertainty, calculated as

$$D_{{\rm stat},ii} = \sigma^2_{\mu_{B,i}}. \tag{3.8}$$

The detailed description and the systematic covariance matrix together with $\mu_{B,i}$, $\sigma^2_{\mu_{B,i}}$, $z_{\rm cmb}$, and $z_{\rm hel}$ for the ith SnIa are mentioned in [150].

3.3 BAO

The completed experiments of the Sloan Digital Sky Survey (SDSS) recently presented the BAO measurements using galaxies, Lyman-α (Lyα), and quasars [154]. These experiments include the compilation of data from SDSS, BOSS, SDSS-II, and eBOSS, offering independent BAO measurements of Hubble distances and angular-diameter distances relative to the sound horizon from eight different samples as shown in Table 3.1.

The comoving size of the sound horizon ($r_{\rm s}$) at the drag redshift ($z_{\rm d}$), i.e., $r_{\rm d}$, is calculated as:

$$r_{\rm d} = r_{\rm s}(z_{\rm d}) = \int_{z_{\rm d}}^{\infty} \frac{c_{\rm s} {\rm d}z}{H(z)}. \tag{3.9}$$

We use the best fit values of $z_{\rm d}$ for the spatially flat and non-flat cases as obtained in [155] for the ΛCDM and $o\Lambda$CDM models, respectively, for the CMB and CMB+Lens cases. For CMB, we use $z_{\rm d} = 1059.971$ in ΛCDM and An-ΛCDM

Table 3.1 : Clustering measurements for the BAO samples.

Parameter	MGS	BOSS Galaxy	BOSS Galaxy	eBOSS LRG	eBOSS ELG	eBOSS Quasar	Lyα-Lyα	Lyα-Quasar
z_{eff}	0.15	0.38	0.51	0.70	0.85	1.48	2.33	2.33
$D_V(z)/r_{\mathrm{d}}$	4.47 ± 0.17	—	—	—	$18.33^{+0.57}_{-0.62}$	—	—	—
$D_M(z)/r_{\mathrm{d}}$	—	10.23 ± 0.17	13.36 ± 0.21	17.86 ± 0.33	—	30.69 ± 0.80	37.6 ± 1.9	37.3 ± 1.7
$D_H(z)/r_{\mathrm{d}}$	—	25.00 ± 0.76	22.33 ± 0.58	19.33 ± 0.53	—	13.26 ± 0.55	8.93 ± 0.28	9.08 ± 0.34

models, and $z_{\mathrm{d}} = 1060.390$ in $o\Lambda$CDM and An-$o\Lambda$CDM models. For CMB+Lens, we consider $z_{\mathrm{d}} = 1059.971$ in ΛCDM and An-ΛCDM models, and $z_{\mathrm{d}} = 1060.123$ in $o\Lambda$CDM and An-$o\Lambda$CDM models. Further, the sound speed of the baryon-photon fluid reads $c_{\mathrm{s}} = \frac{c}{\sqrt{3(1+\mathcal{R})}}$, where $\mathcal{R} = \frac{3\Omega_{\mathrm{b}0}}{4\Omega_{\gamma 0}(1+z)}$ with $\Omega_{\mathrm{b}0} = 0.022h^{-2}$ being the present-day physical density of baryons [156] and $\Omega_{\gamma 0} = 2.469\times10^{-5}h^{-2}$ being the present-day physical density of photons [157–161].

BAO measurements directly constrain the quantities $D_H(z)/r_{\mathrm{d}}$ and $D_M(z)/r_{\mathrm{d}}$. The Hubble distance at redshift z is measured as

$$D_H(z) = \frac{c}{H(z)}. \tag{3.10}$$

The comoving angular diameter distance $D_M(z)$ is calculated as

$$D_M(z) = \frac{c}{H_0} S_k\left(\frac{D_C(z)}{c/H_0}\right), \tag{3.11}$$

where the comoving distance of the line-of-sight is

$$D_C(z) = \frac{c}{H_0}\int_0^z \mathrm{d}z' \frac{H_0}{H(z')}, \tag{3.12}$$

and

$$S_\kappa(x) = \begin{cases} \sin(\sqrt{-\Omega_\kappa}x)/\sqrt{-\Omega_\kappa} & \text{for} \quad \Omega_\kappa < 0, \\ x & \text{for} \quad \Omega_\kappa = 0, \\ \sinh(\sqrt{\Omega_\kappa}x)/\sqrt{\Omega_\kappa} & \text{for} \quad \Omega_\kappa > 0. \end{cases} \tag{3.13}$$

Further, these measurements are summarized by a quantity $D_V(z)/r_{\mathrm{d}}$, with the spherically averaged distance $D_V(z)$ as

$$D_V(z) \equiv \left[zD_M^2(z)D_H(z)\right]^{1/3}. \tag{3.14}$$

We now define the chi-squared function corresponding to each distance considered in Table 3.1. We denote d_1 for $D_V(z)/r_{\mathrm{d}}$, d_2 for $D_M(z)/r_{\mathrm{d}}$, and d_3 for $D_H(z)/r_{\mathrm{d}}$, respectively. The chi-squared function for each measurement is considered as

$$
\begin{aligned}
\chi^2_{\mathrm{B}_1} &= \sum_{i=1}^{2}\left(\frac{d_1^{\mathrm{obs}}(z_i)-d_1^{\mathrm{th}}(z_i)}{\sigma_{d_1^{\mathrm{obs}}(z_i)}}\right)^2,\\
\chi^2_{\mathrm{B}_2} &= \sum_{j=1}^{6}\left(\frac{d_2^{\mathrm{obs}}(z_j)-d_2^{\mathrm{th}}(z_j)}{\sigma_{d_2^{\mathrm{obs}}(z_j)}}\right)^2,\\
\chi^2_{\mathrm{B}_3} &= \sum_{j=1}^{6}\left(\frac{d_3^{\mathrm{obs}}(z_j)-d_3^{\mathrm{th}}(z_j)}{\sigma_{d_3^{\mathrm{obs}}(z_j)}}\right)^2.
\end{aligned}
\tag{3.15}
$$

Here, d^{obs} is the observed distance value as given in Table 3.1, while d^{th} is the theoretical value calculated for the models under consideration. In the case of $D_V(z)/r_{\mathrm{d}}$, z_i $(i=1,2)$ are respectively the effective redshifts for the two measurements of samples, MGS and eBOSS ELG. While, in the case of $D_M(z)/r_{\mathrm{d}}$ and $D_H(z)/r_{\mathrm{d}}$, z_j $(j=1,2,3,4,5,6)$ are respectively the effective redshifts for the six measurements: BOSS Galaxy, BOSS Galaxy, eBOSS Galaxy, eBOSS LRG, eBOSS Quasar, Lyα-Lyα, and Lyα-Quasar.

Thus, the total chi-squared function for the BAO measurements, denoted by χ^2_{BAO}, reads

$$\chi^2_{\mathrm{BAO}} = \chi^2_{\mathrm{B}_1} + \chi^2_{\mathrm{B}_2} + \chi^2_{\mathrm{B}_3}. \tag{3.16}$$

3.4 CMB

In [162], various cosmological models are constrained using the compressed CMB likelihood information. In this approach, CMB measurements are compressed to the variables that govern the expansion history of the universe. The compressed form helps in simplifying the computations, and allows to fit complex models. Here, we follow a similar approach and use the compressed likelihood information of the CMB data from Planck 2018 chains [155] as described in the following.

In the case of CMB data, we fix the photon-decoupling surface $z_* = 1089.920$ for the spatially flat models (ΛCDM and An-ΛCDM), and the chi-squared function denoted by $\chi^2_{\mathrm{C}_1}$, reads as

$$\chi^2_{\mathrm{C}_1} = \Delta p_i {C_1}^{-1} (\Delta p_i)^T, \quad \Delta p_i = p_i^{\mathrm{th}} - p_i^{\mathrm{mean}}, \tag{3.17}$$

where $i=1,2,3$ with $p_1=\omega_{\mathrm{b}}$, $p_2=\omega_{\mathrm{cdm}}$, and $p_3 = 100\theta_{\mathrm{MC}}$. p_i^{mean} are the mean values of the parameters from Planck 2018 chains, and C_1 is the covariance matrix for

$(\omega_{\rm b}, \omega_{\rm cdm}, 100\theta_{\rm MC})$, given by

$$\begin{bmatrix} 2.18\times10^{-8} & -1.16\times10^{-7} & 1.60\times10^{-8} \\ -1.16\times10^{-7} & 1.85\times10^{-6} & -1.41\times10^{-7} \\ 1.60\times10^{-8} & -1.41\times10^{-7} & 9.62\times10^{-8} \end{bmatrix}.$$

Further, we fix $z_* = 1089.411$ for the spatially non-flat models ($o\Lambda$CDM and An-$o\Lambda$CDM), and the chi-squared function denoted by $\chi^2_{\rm C_2}$, reads as

$$\chi^2_{\rm C_2} = \Delta q_i {C_2}^{-1} (\Delta q_i)^T, \quad \Delta q_i = q_i^{\rm th} - q_i^{\rm mean}, \tag{3.18}$$

where $i = 1,2,3,4$ with $q_1 = \omega_{\rm b}$, $q_2 = \omega_{\rm cdm}$, $q_3 = 100\theta_{\rm MC}$ and $q_4 = \Omega_\kappa$. Here $q_i^{\rm mean}$ are the mean values of the parameters from Planck 2018 chains, and C_2 is the covariance matrix for $(\omega_{\rm b}, \omega_{\rm cdm}, 100\theta_{\rm MC}, \Omega_\kappa)$, given by

$$\begin{bmatrix} 2.88\times10^{-8} & -1.68\times10^{-7} & 2.53\times10^{-8} & -1.30\times10^{-6} \\ -1.68\times10^{-7} & 2.18\times10^{-6} & -2.18\times10^{-7} & 1.04\times10^{-5} \\ 2.53\times10^{-8} & -2.18\times10^{-7} & 1.05\times10^{-7} & -1.60\times10^{-6} \\ -1.30\times10^{-6} & 1.04\times10^{-5} & -1.60\times10^{-6} & 2.94\times10^{-4} \end{bmatrix}.$$

Similarly, we evaluate the chi-squared distribution for spatially flat and non-flat models in the case of CMB+Lens data.

In order to constrain the parameters of the models under consideration with different combinations of the aforementioned datasets, we use a Python interface for `Multinest` [163–165], namely the `Pymultinest` code [166]. We further analyze our models with the Bayesian inference tool, nested sampling [167] that helps in model comparison by calculating Bayesian evidence. We define the total multivariate joint Gaussian likelihood function as

$$\mathcal{L}_{\rm tot} \propto \exp\left(\frac{-\chi^2_{\rm tot}}{2}\right), \tag{3.19}$$

where the total chi-square function of all the datasets reads

$$\chi^2_{\rm tot} = \chi^2_{\rm CC} + +\chi^2_{\rm Pan} + \chi^2_{\rm BAO} + \chi^2_{\rm CMB}. \tag{3.20}$$

In our study, we choose uniform prior distribution for all the model parameters, viz., $35 < H_0$ [km s^{-1}Mpc^{-1}] < 85, $0.1 < \Omega_{\rm m0} < 0.7$, $-40 < \log_{10}(\Omega_{\sigma0}) < 0$ [except the analysis for the data sets CC, Pan, and CC+Pan, for which we use $-4 < \log_{10}(\Omega_{\sigma0}) < 0$], and $-0.3 < \Omega_{\kappa0} < 0.3$. [1]

Finally, note that we aim in this study to constrain the allowed amount of expansion anisotropy, quantified by its stiff fluid-like contribution, $\rho_\sigma \propto (1+z)^6$, to the Friedmann equation (2.64), from the observational data on top of the ΛCDM and $o\Lambda$CDM models, and assess its effects (see section 2.5 for more discussion). Notice that $\Omega_{\sigma0}s^{-6}$ is the fastest growing term with decreasing s, i.e., increasing z, in the Friedmann equation. Therefore, we expect to typically achieve constraints getting tighter on $\Omega_{\sigma0}$ as we use data from higher redshifts; as is reflected in the sequence of our discussion in the next section. Also, as the deviations from the isotropic models would be pronounced more and more with increasing redshift, for guaranteeing expansion anisotropy to remain as a correction all the way to the largest redshifts relevant to the CMB and BAO data used in our analyses, we fix the drag redshift $z_{\rm d}$ (involved in the BAO data analyses, see section 3.3) and the last scattering redshift z_* (involved in the CMB data analyses, see section 3.4) for An-$o\Lambda$CDM and An-ΛCDM by using respectively the values obtained for $o\Lambda$CDM and ΛCDM in the Planck 2018 release [155].

[1]In the CMB and BAO data likelihoods, we have used some fixed high redshifts values, viz., the drag redshift $z_{\rm d}$ and the last-scattering redshift z_*, and therefore a small amount of anisotropy is expected in our results, as a correction on the top of standard ΛCDM. The redshift $z \sim 1100$ of recombination where the Universe is supposed to be matter dominated, is physically closely related to z_* and $z_{\rm d}$. Therefore, using $\Omega_{\rm m}(z\sim 1100) \approx 1$ and say, $\Omega_\sigma(z\sim 1100) \lesssim 10^{-2}$ into $\frac{\Omega_\sigma}{\Omega_{\rm m}} = \frac{\Omega_{\sigma0}}{\Omega_{\rm m0}}(1+z)^3$, the upper bound for $\frac{\Omega_{\sigma0}}{\Omega_{\rm m0}}$ is found to be $\sim 10^{-11}$. The test runs of the code suggested that the prior range $-40 < \log_{10}(\Omega_{\sigma0}) < 0$ is good enough to extract the information about $\Omega_{\sigma0}$.

4. RESULTS AND DISCUSSIONS

In this section, we discuss the observational constraints on the cosmological parameters of the models (viz., An-$o\Lambda$CDM described in (2.64) and its particular cases $o\Lambda$CDM, An-ΛCDM, and ΛCDM) obtained by using the data sets from the different observational probes (viz., CC, SnIa Pantheon, BAO, and CMB) and their various combinations, and the methods as discussed in Sec. 3. In Tables 4.1, 4.2, and 4.3, we report the bounds at 68% and 95% Confidence Level (C.L.) for H_0, $\Omega_{\rm m0}$, $\Omega_{\kappa 0}$, and $\log_{10}(\Omega_{\sigma 0})$, while we show the corresponding one and two-dimensional marginalized posteriors in the figures from Figure 4.1 to Figure 4.6.

Table 4.1 displays the constraints on the model parameters from the CC, Pan, and CC+Pan data, which are relatively low redshifts ($z \lesssim 2.4$) data. The accompanying Figure 4.1 compares the constraints of different models for a given data set while Figure 4.2 compares the constraints from different data sets for a given model.

Table 4.1 : Constraints on the An-$o\Lambda$CDM, $o\Lambda$CDM, An-ΛCDM, and ΛCDM model parameters from CC, Pan, and CC+Pan data. The upper bound of $\log_{10}(\Omega_{\sigma 0})$ is at 95% C.L. The parameter H_0 is measured in units of km s^{-1} Mpc^{-1}.

Parameter	CC	Pan	CC+Pan
An-$o\Lambda$CDM			
H_0	$68.2^{+3.1+6.2}_{-3.1-5.8}$	70^{+8+10}_{-8-10}	$69.0^{+1.9+3.8}_{-1.9-3.8}$
$\Omega_{\rm m0}$	$0.302^{+0.081+0.15}_{-0.081-0.15}$	$0.286^{+0.065+0.11}_{-0.065-0.12}$	$0.300^{+0.067+0.11}_{-0.058-0.12}$
$\Omega_{\kappa 0}$	$0.02^{+0.20+0.26}_{-0.16-0.28}$	$-0.01^{+0.14+0.26}_{-0.14-0.26}$	$-0.02^{+0.14+0.26}_{-0.14-0.26}$
$\log_{10}(\Omega_{\sigma 0})$	< -2.23	< -1.77	< -2.22
$o\Lambda$CDM			
H_0	$67.9^{+3.0+6.2}_{-3.0-5.9}$	71^{+9+10}_{-9-10}	$69.1^{+2.0+4.0}_{-2.0-3.9}$
$\Omega_{\rm m0}$	$0.328^{+0.081+0.13}_{-0.072-0.14}$	$0.318^{+0.062+0.10}_{-0.052-0.11}$	$0.321^{+0.062+0.10}_{-0.053-0.11}$
$\Omega_{\kappa 0}$	$0.00^{+0.16+0.28}_{-0.16-0.28}$	$-0.05^{+0.12+0.26}_{-0.16-0.24}$	$-0.05^{+0.13+0.27}_{-0.17-0.24}$
An-ΛCDM			
H_0	$68.1^{+3.0+6.1}_{-3.0-5.7}$	69^{+9+10}_{-10-10}	$68.8^{+1.8+3.6}_{-1.8-3.6}$
$\Omega_{\rm m0}$	$0.311^{+0.064+0.13}_{-0.064-0.13}$	$0.284^{+0.031+0.056}_{-0.025-0.059}$	$0.292^{+0.023+0.045}_{-0.023-0.046}$
$\log_{10}(\Omega_{\sigma 0})$	< -2.22	< -1.80	< -2.19
ΛCDM			
H_0	$67.8^{+2.9+5.6}_{-2.9-5.6}$	70^{+9+10}_{-9-10}	$69.0^{+1.8+3.5}_{-1.8-3.5}$
$\Omega_{\rm m0}$	$0.330^{+0.052+0.12}_{-0.065-0.11}$	$0.298^{+0.022+0.044}_{-0.022-0.041}$	$0.302^{+0.020+0.041}_{-0.021-0.039}$

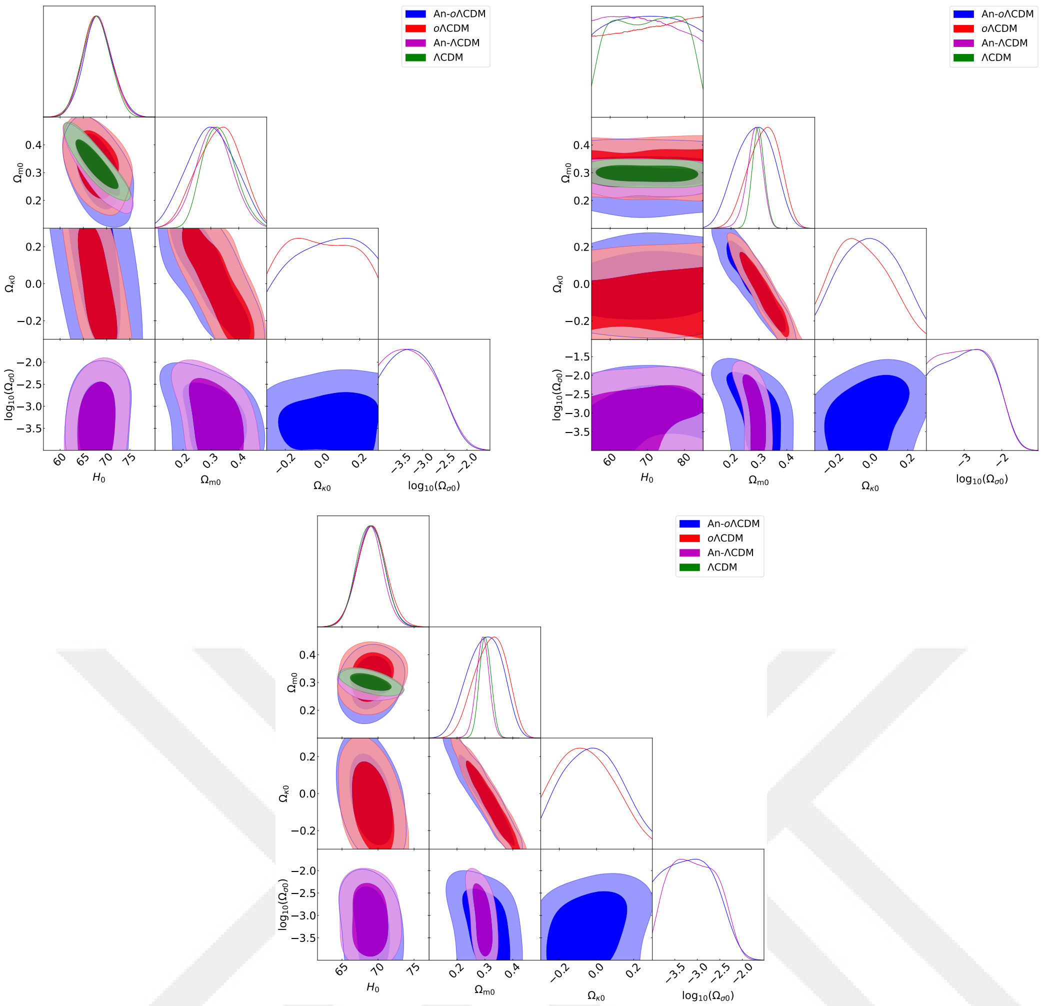

Figure 4.1 : One-dimensional and two-dimensional marginalized confidence regions (68% and 95% C.L.) from CC (top-left), Pan (top-right), and CC+Pan (bottom) data for An-$o\Lambda$CDM, $o\Lambda$CDM, An-ΛCDM, and ΛCDM model parameters. The parameter H_0 is measured in units of km s^{-1} Mpc^{-1}.

We notice that, regardless of whether or not anisotropic expansion is allowed, the CC data set constrains H_0 better than $\Omega_{\kappa0}$, while the Pan data set constrains $\Omega_{\kappa0}$ better than H_0. The combination of CC and Pan data provides stronger constraints on the parameters of the models in general, but constraints on the expansion anisotropy, viz., $\Omega_{\sigma0}$, are not affected significantly, see Figure 4.2. When we use only the CC data or Pantheon 2018 data, or the combination of these two, the upper bounds on the expansion anisotropy are allowed to be large; up to $\log_{10}(\Omega_{\sigma0}) < -1.77$ at 95% C.L. (An-$o\Lambda$CDM with Pan). The tightest upper bound is $\log_{10}(\Omega_{\sigma0}) < -2.23$ at 95% C.L. (An-$o\Lambda$CDM with CC) and it is slightly looser than those obtained from the model independent constraints, e.g., from the SnIa data, $\log_{10}(\Omega_{\sigma0}) \lesssim -3$ assuming LRS Bianchi type I background [107–113]. We notice that the models with spatial curvature are predicted to be well consistent with the spatially flat ($\Omega_{\kappa0} = 0$) models in all these

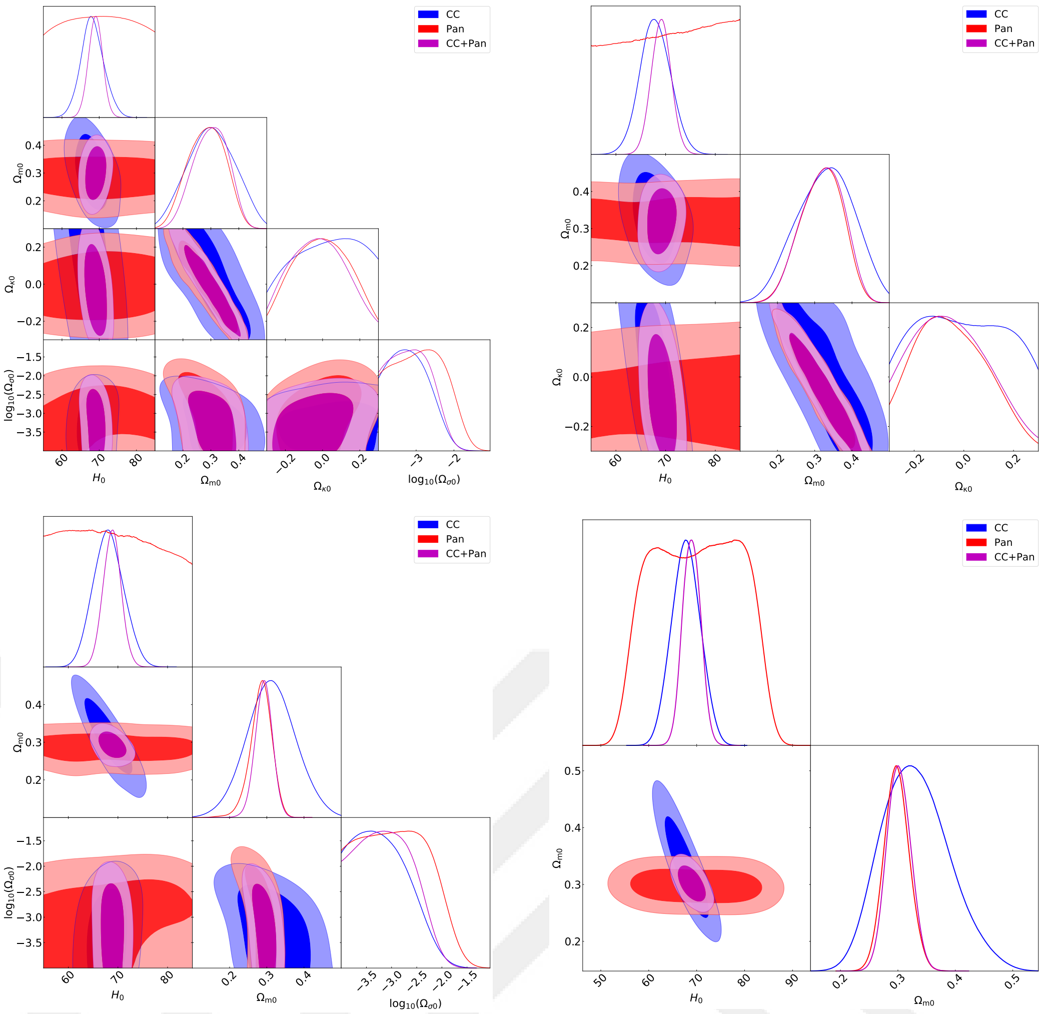

Figure 4.2 : One-dimensional and two-dimensional marginalized confidence regions (68% and 95% C.L.) of An-$o\Lambda$CDM (top-left), $o\Lambda$CDM (top-right), An-ΛCDM (bottom-left), and ΛCDM (bottom-right) model parameters from CC, Pan and CC+Pan data combinations. The parameter H_0 is measured in units of km s^{-1} Mpc^{-1}.

analyses. We find no significant difference among the predicted H_0 values, yet, it might be interesting to notice that the introduction of expansion anisotropy leads to a slight increase in the predicted mean value of H_0 for the CC data and to a slight decrease in it for the Pan data. Also, for these cases, the introduction of spatial curvature does not change the constraints of the parameters, because these models are predicted to be well consistent with a spatially flat universe.

Table 4.2 displays the constraints from the BAO data combined with the Pantheon 2018 data and from the CMB data (alone and in combination with the Pantheon 2018 data). We see that including the BAO data from the measurements at redshifts up to $z = 2.33$ (see Table 3.1)—but carry information from much higher redshifts via the

Table 4.2 : Constraints on the An-$o\Lambda$CDM, $o\Lambda$CDM, An-ΛCDM, and ΛCDM model parameters from BAO+Pan, CMB only, and CMB+Pan data. The upper bound of $\log_{10}(\Omega_{\sigma 0})$ is at 95% C.L. The parameter H_0 is measured in units of km s^{-1} Mpc^{-1}.

Parameter	BAO+Pan	CMB	CMB+Pan
An-$o\Lambda$CDM			
H_0	$67.3^{+2.9+6.6}_{-3.5-6.1}$	$54.2^{+2.9+7}_{-3.5-6}$	$66.7^{+2.2+5.2}_{-2.6-4.6}$
$\Omega_{\rm m0}$	$0.294^{+0.027+0.054}_{-0.027-0.049}$	$0.484^{+0.056+0.12}_{-0.056-0.11}$	$0.319^{+0.023+0.045}_{-0.023-0.0446}$
$\Omega_{\kappa 0}$	$0.013^{+0.074+0.15}_{-0.074-0.15}$	$-0.046^{+0.017+0.029}_{-0.014-0.032}$	$-0.0032^{+0.0059+0.011}_{-0.0059-0.012}$
$\log_{10}(\Omega_{\sigma 0})$	< -14.3	< -16.3	< -17.1
$o\Lambda$CDM			
H_0	$67.4^{+3.0+7.2}_{-3.5-6.3}$	$54.3^{+2.6+7}_{-3.9-6}$	$66.7^{+2.5+5.1}_{-2.5-4.8}$
$\Omega_{\rm m0}$	$0.294^{+0.027+0.054}_{-0.027-0.055}$	$0.483^{+0.058+0.11}_{-0.058-0.12}$	$0.320^{+0.023+0.047}_{-0.025-0.045}$
$\Omega_{\kappa 0}$	$0.010^{+0.076+0.15}_{-0.076-0.15}$	$-0.045^{+0.016+0.031}_{-0.016-0.031}$	$-0.0032^{+0.0068+0.011}_{-0.0056-0.013}$
An-ΛCDM			
H_0	$67.7^{+1.2+2.7}_{-1.5-2.6}$	$67.57^{+0.64+1.3}_{-0.64-1.3}$	$67.75^{+0.60+1.2}_{-0.60-1.2}$
$\Omega_{\rm m0}$	$0.297^{+0.014+0.029}_{-0.014-0.028}$	$0.3125^{+0.0085+0.017}_{-0.0085-0.017}$	$0.3102^{+0.0078+0.016}_{-0.0078-0.015}$
$\log_{10}(\Omega_{\sigma 0})$	< -14.3	< -17.9	< -17.2
ΛCDM			
H_0	$67.6^{+1.3+2.7}_{-1.3-2.5}$	$67.59^{+0.65+1.3}_{-0.65-1.3}$	$67.75^{+0.64+1.2}_{-0.64-1.2}$
$\Omega_{\rm m0}$	$0.297^{+0.014+0.029}_{-0.014-0.027}$	$0.3122^{+0.0087+0.017}_{-0.0087-0.017}$	$0.3100^{+0.0084+0.017}_{-0.0084-0.015}$

drag redshift $z_{\rm d} \sim 1060$ information—in our analyses with low-redshift data, viz., Pan, improves the constraints on the expansion anisotropy term considerably, as expected; see also the accompanying figures, viz., Figure 4.3 and Figure 4.4. Accordingly, when the CMB data set is not in the picture, the most stringent upper bound on the expansion anisotropy is obtained by the BAO+Pan data, which is $\log_{10}(\Omega_{\sigma 0}) < -14.3$ at 95% C.L. irrespective of the presence of spatial curvature, as the cases with spatial curvature are predicted to be well consistent with a spatially flat universe. However we notice that, for the models with spatial curvature, the data predict slightly lower mean values for H_0 accompanied by a slight tendency towards a spatially open universe, which can be associated with the negative correlation between H_0 and $\Omega_{\kappa 0}$, see the top-left panel of Figure 4.3. As discussed above, we expect to achieve the tightest constraints on the expansion anisotropy when the CMB information, the data relevant to the highest redshifts ($z \sim 1100$) among the data sets we used, is included in our analyses. We notice that the constraints, both for the ΛCDM and $o\Lambda$CDM models, are in exquisite agreement with those obtained by the Planck collaboration [4]. We find that the H_0 predicted by the ΛCDM model with the CMB data only is in tension with the local measurements of H_0 [104–106], and this tension reaches a level more than 5σ

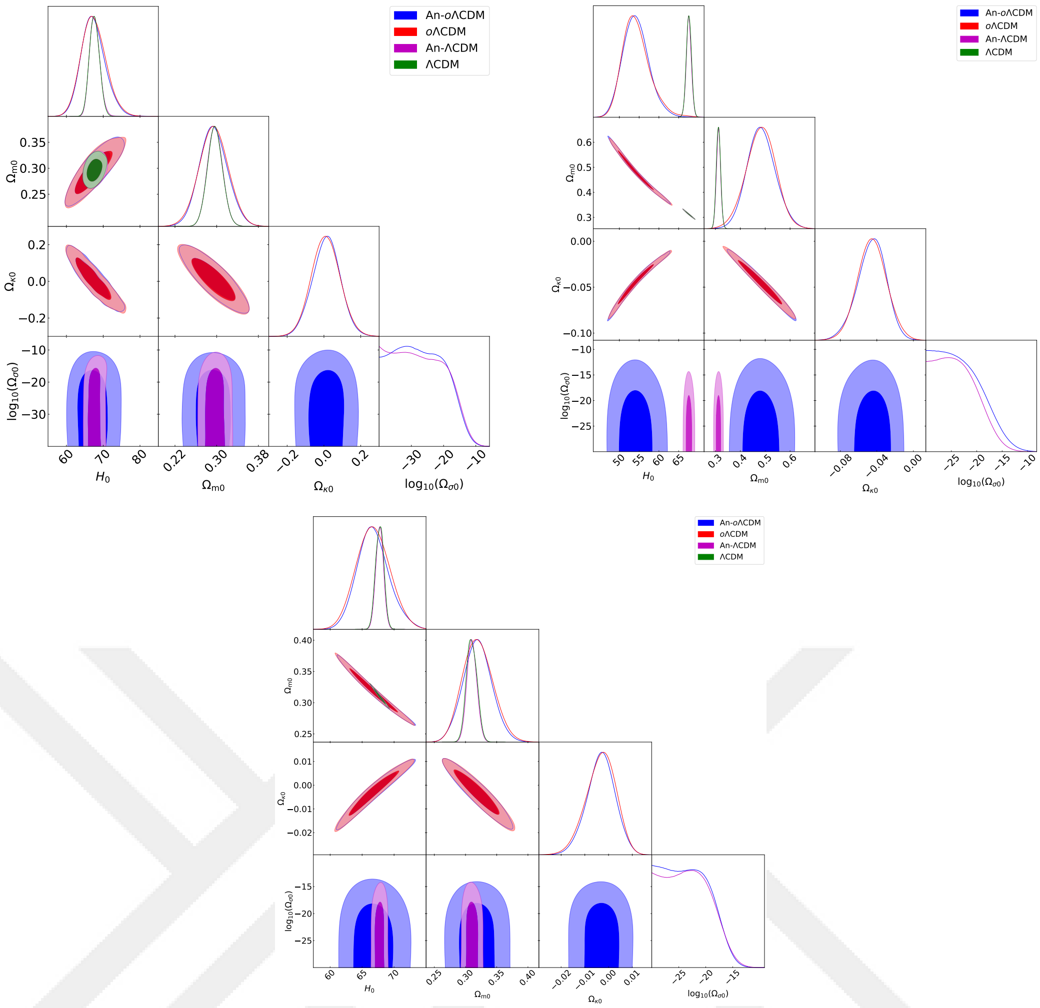

Figure 4.3 : One-dimensional and two-dimensional marginalized confidence regions (68% and 95% C.L.) from BAO+Pan (top-left), CMB (top-right) and CMB+Pan (bottom) data for An-$o\Lambda$CDM, $o\Lambda$CDM, An-ΛCDM, and ΛCDM model parameters. The parameter H_0 is measured in units of km s^{-1} Mpc^{-1}.

with the SH0ES collaboration measurements, where the latest estimation reads $H_0 = 73.04 \pm 1.04\,\mathrm{km\,s^{-1}\,Mpc^{-1}}$ [104]. Moreover, we notice that this tension is exacerbated by the introduction of spatial curvature, i.e., in the $o\Lambda$CDM model, see Table 4.2 and the top-right panel of Figure 4.3. This gives evidence for a spatially closed universe at more than 3σ level while lowering the predicted Hubble constant value [19, 20]. The introduction of the expansion anisotropy, i.e., the An-$o\Lambda$CDM and the An-ΛCDM models, does not modify these findings, as can be seen from the top-right panel of Figure 4.3. This happens because, as can be seen from the same panel, within 2σ, the CMB data set by alone already predicts that the anisotropic models, An-$o\Lambda$CDM and An-ΛCDM, remain consistent with their isotropic ($\Omega_{\sigma 0} = 0$) counterparts, $o\Lambda$CDM and ΛCDM. However, the introduction of spatial curvature relaxes the upper bound

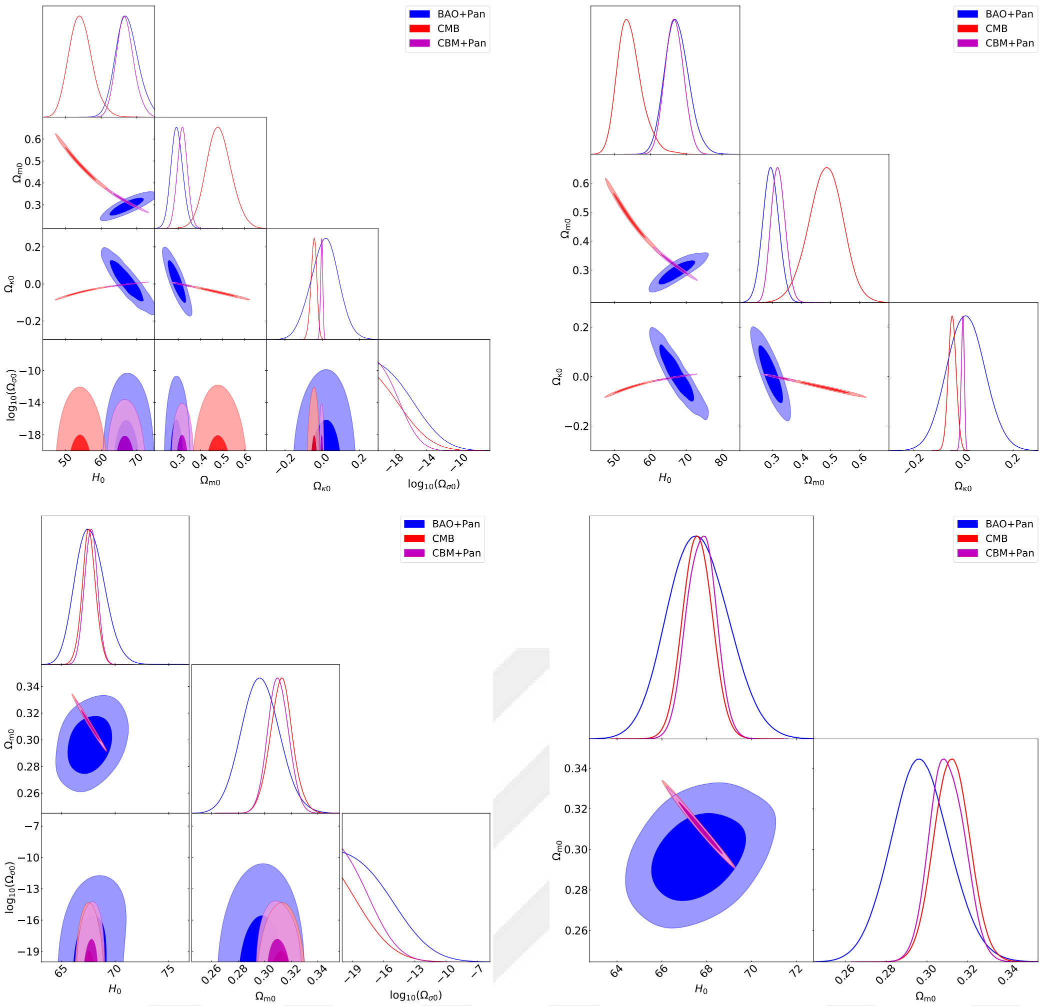

Figure 4.4 : One-dimensional and two-dimensional marginalized confidence regions (68% and 95% C.L.) of An-$o\Lambda$CDM (top-left), $o\Lambda$CDM (top-right), An-ΛCDM (bottom-left), and ΛCDM (bottom-right) model parameters from BAO+Pan, CMB and CMB+Pan data combinations. The parameter H_0 is measured in units of km s^{-1} Mpc^{-1}.

on $\Omega_{\sigma0}$ obtained for the An-ΛCDM model; namely, the constraint on the expansion anisotropy relaxes from $\log_{10}(\Omega_{\sigma0}) < -17.9$ (95% C.L.) of the An-ΛCDM model to $\log_{10}(\Omega_{\sigma0}) < -16.3$ (95% C.L.) of the An-$o\Lambda$CDM model (see also the top-right panel of Figure 4.3). The inclusion of the Pantheon 2018 data in our CMB data only analyses, improves the determination of the parameters by breaking their correlations; in particular, in the models with spatial curvature (see top panels in Figure 4.4 and also the bottom panel of Figure 4.3). The introduction of the spatial curvature on top of ΛCDM or An-ΛCDM in this case (CMB+Pan) does not affect the results as now $\Omega_{\kappa0}$ is well constrained and is in good agreement with a spatially flat ($\Omega_{\kappa0} = 0$) universe, see bottom panel of Figure 4.3. Therefore, the upper bound on the expansion anisotropy remains almost unaltered, viz., $\log_{10}(\Omega_{\sigma 0}) < -17.1$ for An-$o\Lambda$CDM and $\log_{10}(\Omega_{\sigma 0}) < -17.2$ for An-ΛCDM, both at 95% C.L.

It is well known that the prediction of spatially closed background by $o\Lambda$CDM with the CMB only data is accompanied by substantially higher lensing amplitudes compared to ΛCDM, and that combining the CMB data with the lensing reconstruction (which is consistent with spatial flatness) pulls the parameters of $o\Lambda$CDM back into consistency with a spatially flat background within 2σ [4]. Also, whereas the addition of CMB lensing with the CMB data weakly breaks the geometric degeneracy regarding spatial curvature, the spatial flatness can be tested to high accuracy by adding the BAO data. Therefore, in Table 4.3, we present first the constraints from the combined data sets CMB+Lens and CMB+Lens+BAO, and then from the data combinations obtained by adding astrophysical data sets, namely, Pantheon 2018 and CC; see also the accompanying figures, viz., Figure 4.5 and Figure 4.6.

Table 4.3 : Constraints on the An-$o\Lambda$CDM, $o\Lambda$CDM, An-ΛCDM, and ΛCDM model parameters from CMB+Lens, CMB+Lens+BAO, CMB+Lens+Pan, CMB+Lens+BAO+Pan, and CMB+Lens+BAO+Pan+CC data. The upper bound of $\log_{10}(\Omega_{\sigma 0})$ is at 95% C.L. The parameter H_0 is measured in units of km s^{-1} Mpc^{-1}.

Parameter	CMB+Lens	CMB+Lens+BAO	CMB+Lens+Pan	CMB+Lens+BAO+Pan	CMB+Lens+BAO+Pan+CC
An-$o\Lambda$CDM					
H_0	$63.8^{+2.0+4.3}_{-2.2-4.2}$	$67.71^{+0.66+1.3}_{-0.66-1.3}$	$66.2^{+1.8+4.0}_{-2.0-3.6}$	$67.78^{+0.65+1.3}_{-0.65-1.3}$	$67.85^{+0.62+1.2}_{-0.62-1.2}$
Ω_{m0}	$0.347^{+0.022+0.043}_{-0.022-0.043}$	$0.3093^{+0.0063+0.013}_{-0.0063-0.012}$	$0.323^{+0.017+0.034}_{-0.017-0.035}$	$0.3086^{+0.0061+0.012}_{-0.0061-0.012}$	$0.3082^{+0.0059+0.012}_{-0.0059-0.011}$
$\Omega_{\kappa 0}$	$-0.0107^{+0.0062+0.012}_{-0.0062-0.012}$	$-0.0006^{+0.0021+0.0040}_{-0.0021-0.0040}$	$-0.0045^{+0.0050+0.0097}_{-0.0050-0.010}$	$-0.0005^{+0.0020+0.0040}_{-0.0020-0.0040}$	$-0.0002^{+0.0019+0.0038}_{-0.0019-0.0037}$
$\log_{10}(\Omega_{\sigma 0})$	< -17.7	< -17.5	< -17.6	< -17.4	< -17.1
$o\Lambda$CDM					
H_0	$63.9^{+2.1+4.7}_{-2.4-4.2}$	$67.69^{+0.65+1.3}_{-0.65-1.3}$	$66.2^{+1.9+3.6}_{-1.9-3.5}$	$67.80^{+0.66+1.3}_{-0.66-1.2}$	$67.86^{+0.60+1.2}_{-0.60-1.2}$
Ω_{m0}	$0.346^{+0.023+0.046}_{-0.023-0.045}$	$0.3096^{+0.0062+0.012}_{-0.0062-0.012}$	$0.323^{+0.017+0.034}_{-0.017-0.032}$	$0.3085^{+0.0062+0.012}_{-0.0062-0.012}$	$0.3081^{+0.0058+0.011}_{-0.0058-0.011}$
$\Omega_{\kappa 0}$	$-0.0103^{+0.0066+0.012}_{-0.0066-0.013}$	$-0.0005^{+0.0020+0.0039}_{-0.0020-0.0039}$	$-0.0043^{+0.0050+0.0093}_{-0.0050-0.0099}$	$-0.0004^{+0.0021+0.0040}_{-0.0021-0.0042}$	$-0.0001^{+0.0020+0.0038}_{-0.0020-0.0038}$
An-ΛCDM					
H_0	$67.67^{+0.58+1.2}_{-0.58-1.1}$	$67.85^{+0.43+0.83}_{-0.43-0.80}$	$67.78^{+0.55+1.1}_{-0.55-1.1}$	$67.90^{+0.42+0.83}_{-0.42-0.81}$	$67.92^{+0.42+0.85}_{-0.42-0.79}$
Ω_{m0}	$0.3110^{+0.0076+0.015}_{-0.0076-0.015}$	$0.3087^{+0.0056+0.010}_{-0.0056-0.011}$	$0.3096^{+0.0072+0.014}_{-0.0072-0.014}$	$0.3080^{+0.0054+0.011}_{-0.0054-0.010}$	$0.3078^{+0.0054+0.010}_{-0.0054-0.010}$
$\log_{10}(\Omega_{\sigma 0})$	< -17.9	< -17.8	< -17.7	< -17.1	< -17.4
ΛCDM					
H_0	$67.63^{+0.58+1.1}_{-0.58-1.1}$	$67.84^{+0.43+0.83}_{-0.43-0.84}$	$67.77^{+0.56+1.1}_{-0.56-1.1}$	$67.89^{+0.43+0.84}_{-0.43-0.83}$	$67.89^{+0.43+0.82}_{-0.43-0.83}$
Ω_{m0}	$0.3116^{+0.0075+0.015}_{-0.0075-0.015}$	$0.3087^{+0.0055+0.011}_{-0.0055-0.010}$	$0.3097^{+0.0073+0.015}_{-0.0073-0.014}$	$0.3081^{+0.0055+0.011}_{-0.0055-0.011}$	$0.3081^{+0.0055+0.011}_{-0.0055-0.010}$

We find that the constraints obtained here for the ΛCDM and $o\Lambda$CDM models are in excellent agreement with those obtained by the Planck collaboration [4]. We observe that the results in Table 4.3 confirm the aforementioned points regarding ΛCDM and $o\Lambda$CDM, and the introduction of the expansion anisotropy does not change the picture; the inclusion of the Lens data to our CMB analyses (CMB+Lens) pulls the parameters of both the An-$o\Lambda$CDM and $o\Lambda$CDM models back into consistency

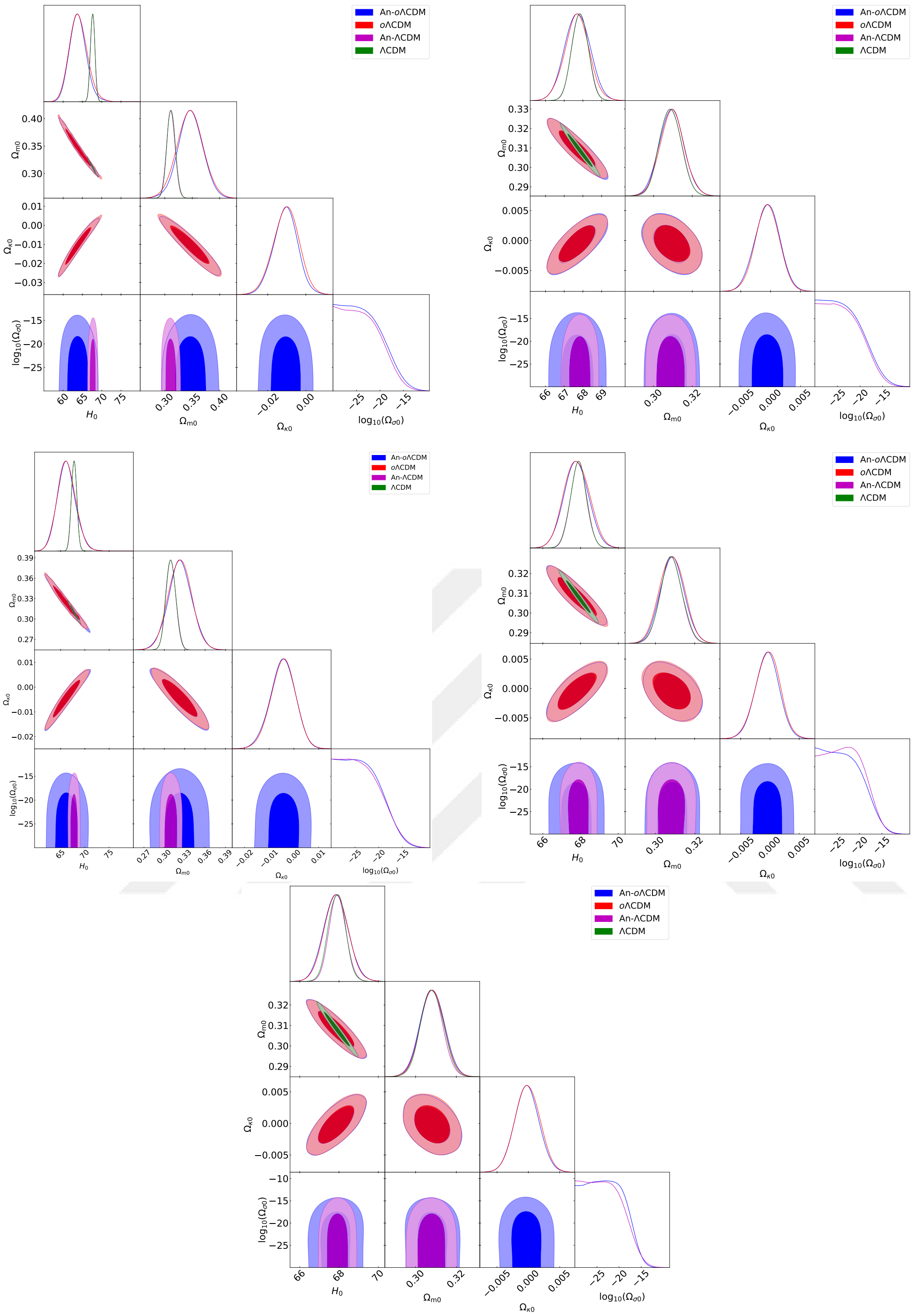

Figure 4.5 : One-dimensional and two-dimensional marginalized confidence regions (68% and 95% C.L.) from CMB+Lens (top-left), CMB+Lens+BAO (top-right), CMB+Lens+Pan (middle-left), CMB+Lens+BAO+Pan (middle-right), and CMB+Lens+BAO+Pan+CC (bottom) data for An-$o\Lambda$CDM, $o\Lambda$CDM, An-ΛCDM, and ΛCDM model parameters. The parameter H_0 is measured in units of km s^{-1} Mpc^{-1}.

with their spatially flat counterparts (An-ΛCDM and ΛCDM) within 2σ, and that the inclusion of the BAO data further tightens the constraints to bring the said consistency

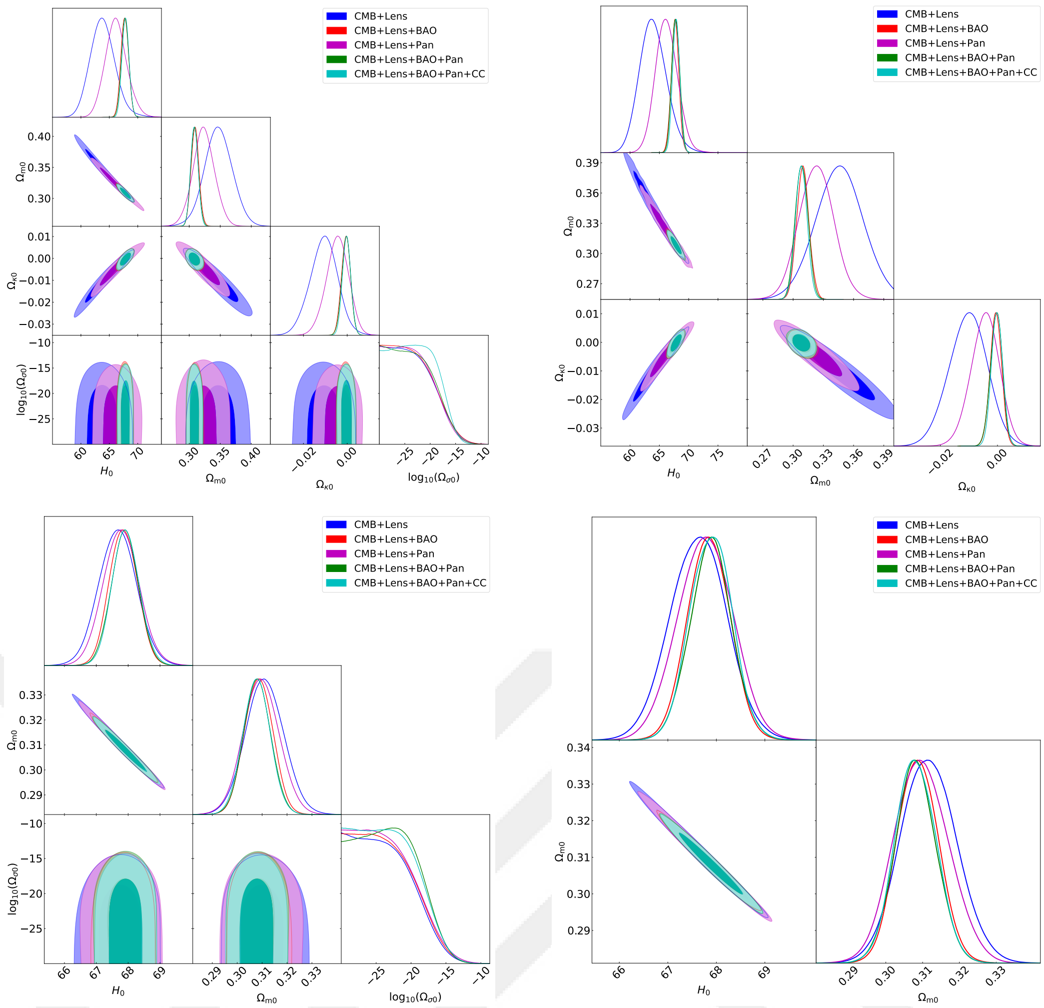

Figure 4.6 : One-dimensional and two-dimensional marginalized confidence regions (68% and 95% C.L.) of An-$o\Lambda$CDM (top-left), $o\Lambda$CDM (top-right), An-ΛCDM (bottom-left) and ΛCDM (bottom-right) model parameters from CMB+Lens, CMB+Lens+BAO, CMB+Lens+Pan, CMB+Lens+BAO+Pan, and CMB+Lens+BAO+Pan+CC data combinations. The parameter H_0 is measured in units of km s^{-1} Mpc^{-1}.

with spatial flatness even below 1σ (see also the top panels of Figure 4.6). We notice positive correlation between H_0 and $\Omega_{\kappa0}$ for all of the combinations of the data sets see also Figure 4.6); the mean values of H_0 typically tend to smaller values accompanied by the slightly negative mean values of $\Omega_{\kappa0}$, and this situation is the most pronounced in the cases of CMB+Lens and CMB+Lens+Pan. With the inclusion of the BAO data—i.e., in the cases of CMB+Lens+BAO, CMB+Lens+BAO+Pan, and CMB+Lens+BAO+Pan+CC—$\Omega_{\kappa0}$ is predicted to be zero with a precision level of $\sim 2\times10^{-3}$. We notice that the introduction of the expansion anisotropy does not change the results (see Figure 4.5); at 95% C.L., the upper bounds on the present-day expansion anisotropy remain stable for the different combinations of data sets, namely, between $\log_{10}(\Omega_{\sigma 0}) < -17.9$ (CMB+Lens) and $\log_{10}(\Omega_{\sigma 0}) < -17.1$ (CMB+Lens+BAO+Pan) for the An-ΛCDM model, and get slightly weakened when non-zero spatial curvature is allowed, between $\log_{10}(\Omega_{\sigma 0}) < -17.7$ (CMB+Lens) and $\log_{10}(\Omega_{\sigma 0}) < -17.1$ (CMB+Lens+BAO+Pan+CC) for the An-$o\Lambda$CDM model (see Figure 4.6). We observe that the inclusion of the data sets BAO, Pan, CC or their combinations in the analyses with the CMB+Lens data does not improve the constraints on the expansion anisotropy rather it slightly relaxes the upper bounds on it (see Figure 4.6). Also, irrespective of the introduction of the spatial curvature, even the loosest upper bound on expansion anisotropy, $\Omega_{\sigma 0} \lesssim 10^{-17}$ at 95% C.L. (CMB+Lens+BAO+Pan+CC), obtained in our analyses with the CMB+Lens data is about two orders of magnitude tighter than $\Omega_{\sigma 0} \lesssim 10^{-15}$, obtained in Ref. [103] for the An-ΛCDM model by using the CMB information along with the $H(z)$, BAO, and Pantheon data. With regard to the H_0 tension, it was reported in Ref. [103] that the predicted mean values of H_0 in the case of the An-ΛCDM model are systematically larger compared to the ΛCDM model, though not significantly. However, with the tighter constraints on the expansion anisotropy found in the current work, it has almost no effect on the predicted H_0 value compared to the ΛCDM model. Thus, we conclude that the introduction of expansion anisotropy on top of the standard ΛCDM model, or its extension allowing spatial curvature as well, does not offer a possible relaxation to the so-called H_0 tension; at least, through its stiff fluid-like contribution to the Friedmann equation.[1]

Finally, in order to compare the goodness of the statistical fits of the models, we calculate their Bayesian evidences. To compare a model $\mathcal{M}_a$ with a reference model $\mathcal{M}_b$, we compute the ratio of the posterior probabilities of the models, given by

$$\frac{P(\mathcal{M}_a|D)}{P(\mathcal{M}_b|D)} = B_{ab}\frac{P(\mathcal{M}_a)}{P(\mathcal{M}_b)}, \tag{4.1}$$

where B_{ab} is the Bayes' factor given by

$$B_{ab} = \frac{\mathcal{E}(D|\mathcal{M}_a)}{\mathcal{E}(D|\mathcal{M}_b)} \equiv \frac{\mathcal{E}_a}{\mathcal{E}_b}. \tag{4.2}$$

[1]However, it is important to recall here that we have limited our investigations to orthogonal (non-tilted) models; otherwise it is possible to arrive at completely different conclusions, see, e.g., Refs. [92–94] as well as Sec. 1 for a discussion and further references on this matter.

The Bayes' factor provides the strength of evidence according to Jeffreys' scale [168], viz., it is weak or inconclusive for $|\ln B_{ab}| \in [0,1)$, definite or positive for $|\ln B_{ab}| \in [1,3)$, strong for $|\ln B_{ab}| \in [3,5)$, and very strong for $|\ln B_{ab}| > 5$. Here, we choose the $o\Lambda$CDM and ΛCDM models as the reference models for the An-$o\Lambda$CDM and An-ΛCDM models, respectively. This is because we have used the compressed CMB likelihood information from the Planck chains for the flat and non-flat ΛCDM models separately in our observational analyses. In Table 4.4, we show Bayesian evidences as well as chi-squared minimum differences, where

$$\begin{aligned}
\Delta \ln B_{o\mathrm{A}} &= \ln \mathcal{E}_{o\Lambda\mathrm{CDM}} - \ln \mathcal{E}_{\mathrm{An}-o\Lambda\mathrm{CDM}}, \\
\Delta \chi^2_{o\mathrm{A}} &= \chi^2_{\min,o\Lambda\mathrm{CDM}} - \chi^2_{\min,\mathrm{An}-o\Lambda\mathrm{CDM}}, \\
\Delta \ln B_{\Lambda\mathrm{A}} &= \ln \mathcal{E}_{\Lambda\mathrm{CDM}} - \ln \mathcal{E}_{\mathrm{An}-\Lambda\mathrm{CDM}}, \\
\Delta \chi^2_{\Lambda\mathrm{A}} &= \chi^2_{\min,\Lambda\mathrm{CDM}} - \chi^2_{\min,\mathrm{An}-\Lambda\mathrm{CDM}}.
\end{aligned}$$

Table 4.4 : Bayesian evidences and chi-squared minimum differences. Here, $\Delta \ln B_{o\mathrm{A}} = \ln \mathcal{E}_{o\Lambda\mathrm{CDM}} - \ln \mathcal{E}_{\mathrm{An}-o\Lambda\mathrm{CDM}}$, $\Delta \chi^2_{o\mathrm{A}} = \chi^2_{\min,o\Lambda\mathrm{CDM}} - \chi^2_{\min,\mathrm{An}-o\Lambda\mathrm{CDM}}$, $\Delta \ln B_{\Lambda\mathrm{A}} = \ln \mathcal{E}_{\Lambda\mathrm{CDM}} - \ln \mathcal{E}_{\mathrm{An}-\Lambda\mathrm{CDM}}$, and $\Delta \chi^2_{\Lambda\mathrm{A}} = \chi^2_{\min,\Lambda\mathrm{CDM}} - \chi^2_{\min,\mathrm{An}-\Lambda\mathrm{CDM}}$.

	$\Delta \ln B_{o\mathrm{A}}$	$\Delta \chi^2_{o\mathrm{A}}$	$\Delta \ln B_{\Lambda\mathrm{A}}$	$\Delta \chi^2_{\Lambda\mathrm{A}}$
CMB	0.72	-0.04	0.86	0.01
CMB+Pan	0.60	0.03	0.57	0.08
CC	0.86	-0.08	0.78	-0.02
Pan	-0.02	0.41	0.72	0.35
CC+Pan	0.46	0.08	0.37	0.06
BAO+Pan	0.17	-0.09	0.33	0.00
CMB+Lens	0.61	0.12	0.29	-0.02
CMB+Lens+BAO	0.57	0.13	0.54	0.05
CMB+Lens+Pan	0.54	0.15	0.54	-0.04
CMB+Lens+BAO+Pan	0.52	-0.15	0.53	0.05
CC+CMB+Lens+BAO+Pan	0.74	0.20	0.52	-0.08

In all of the cases, we notice that the strength of evidence is weak or inconclusive. It is also consistent with the chi-squared minimum differences. It implies that the amount of anisotropic expansion obtained in our analyses is very much allowed on top of the ΛCDM and $o\Lambda$CDM models by the observational data under consideration.

5. CONCLUSIONS

In this work, we have presented an exploration of the possible advantages of the pure geometric extension of the ΛCDM model, which is strongly motivated by the fact that (i) it implies using more realistic spatial backgrounds than that of the spatially flat and maximally symmetric spacetime, and (ii) it is the only way to generalize the ΛCDM model without touching the physics that underpins this model. Accordingly, to begin with, we have replaced, in the simplest manner, the spatially flat RW spacetime assumption of the ΛCDM model with the simplest more realistic background that simultaneously allows non-zero spatial curvature and anisotropic expansion; namely, considered the simplest anisotropic generalizations of the RW spacetime, viz., the Bianchi types I, V, and IX spacetimes (having the simplest homogeneous and flat, open, and closed spatial sections, respectively) combined in one Friedmann equation (2.64). We have then aimed to investigate whether the observational data still support spatial flatness and/or isotropic expansion in this case, and, if not, to explore the roles of spatial curvature and expansion anisotropy (viz., the shear scalar due to its stiff fluid-like behavior) in addressing some of the current cosmological tensions associated with the ΛCDM model [7–11]. We have presented the theoretical background and explicit mathematical construction of this model, dubbed An-oΛCDM, in Sec. 2. We have carried out the analyses of the model, and its particular cases, namely, An-ΛCDM (allowing anisotropic expansion), oΛCDM (allowing non-zero spatial curvature), and ΛCDM, by using the latest data sets from the different observational probes, viz., CC, SnIa Pantheon 2018, BAO, and Planck CMB(+Lens); see Sec. 3 for the data sets and the methodology used, and Sec. 4 for the results (summarized in Tables 4.1, 4.2, and 4.3 and the figures from Figure 4.1 to Figure 4.6) and discussions.

We have found some deviations from spatial flatness and only upper bounds on anisotropic expansion, which also affect the predicted Hubble constant and present-day density parameter of the pressureless fluid, at various significance levels depending on the data set used. However, when the data sets relevant to the low- and high-redshifts are simultaneously employed, all the extended models are predicted to be indistinguishable from the Planck 2018 ΛCDM model [4], though we emphasize that when the spatial curvature is free to vary, some tensions appear between the data [19, 20, 22]. In particular, with regard to the expansion anisotropy, from the low redshift data, viz., the CC and/or Pan data, we have found $\Omega_{\sigma 0} \lesssim 10^{-2}$ (about one order of magnitude looser than the model independent estimations [107–113]), while it considerably tightens to $\Omega_{\sigma 0} \lesssim 10^{-14}$ with the addition of the BAO data. We have obtained the tightest constraints, $\Omega_{\sigma 0} \lesssim 10^{-18}$, when the data set relevant to the highest redshifts ($z \sim 1100$), viz., the CMB(+Lens) information is considered in our analyses. Yet, a very small amount of expansion anisotropy in the late universe cannot be excluded; we have not observed a correlation between $\Omega_{\sigma 0}$ and the other cosmological parameters, and therefore the inclusion of expansion anisotropy does not modify their constraints. These conclusions are well supported by the χ^2 and model comparison analysis (see Table 4.4).

The main lessons that we have learned from this study, which considers the simplest extension of ΛCDM that simultaneously allows non-zero spatial curvature and anisotropic expansion, are summarized as follows:

- The combination at the face value of the current observational data, forgetting about their tension, confirm the spatial flatness and isotropic expansion assumptions of the ΛCDM model, yet a very small amount of expansion anisotropy in the late universe cannot be excluded.
- The introduction of the spatial curvature or the expansion anisotropy, or both, in the simplest manner, on top the ΛCDM model does not offer a possible relaxation to the H_0 tension.
- The introduction of the anisotropic expansion in the simplest manner neither affects the closed space prediction from the CMB data only analyses, nor does improve the drastically reduced value of H_0 which is known to be led by a closed universe (see for example [4, 19, 20]).

Finally, we emphasize that our conclusions (with $\Omega_{\sigma 0} \lesssim 10^{-18}$), which favor the standard ΛCDM model, are based on our observational analysis of the model at the background level using the compressed CMB data. It is conceivable that these will be more pronounced with the already existing stronger upper bounds on the expansion anisotropy ($\Omega_{\sigma 0} \lesssim 10^{-21}$–$10^{-23}$) from the full Planck CMB temperature and polarization spectra measurements [119–121], and the BBN light element abundances [103,118,122,123], because of the absence of correlation between $\Omega_{\sigma 0}$ and the other cosmological parameters. Therefore, we can conclude that the pure geometric extension of the standard ΛCDM model is not helpful in dealing with the cosmological tensions, and the solutions should be sought in possible systematic errors or new physics. However, one should be careful while deriving conclusions from the current work; our findings may also be suggesting further exploration of the role of anisotropic expansion in reaching a successful alternative to ΛCDM. We have studied an extension of ΛCDM obtained by considering only the simplest anisotropic generalizations of the RW spacetime, viz., the Bianchi types I, V, and IX spacetimes (among the spatially homogeneous but not necessarily isotropic spacetimes; the Bianchi spacetimes and Kantowski-Sachs spacetime [31, 32]) combined in one Friedmann equation (2.64) and then treated the shear scalar as a stiff fluid like correction to the usual the FLRW model, thereby, ignored the line of sight of the data in the sky in our analyses. On the other hand, it was suggested in [95] that, even within the simplest anisotropic extension of ΛCDM (using LRS Bianchi type I spacetime, which describes spatially flat but ellipsoidal universe), the H_0 tension can be addressed when the comoving angular diameter distance is allowed to be direction dependent, and additionally, the S_8 tension can be addressed when producing large-scale CMB E-mode correlations via anisotropic expansion is allowed. More importantly, we have limited our investigations to orthogonal (non-tilted) models, yet it is possible to consider tilted models; it is possible to arrive at completely different conclusions through this possibility such as addressing the H_0 tension, but, which could go as far as describing the universe we live in by a tilt and anisotropy on top of Einstein-de Sitter (suggesting that the accelerated late universe is a misinterpretation of the data) [79–102] (see also Refs. [11, 12] for recent reviews). Having said that, such models bring in additional free parameters to be constrained and require investigation by using the full likelihood of the data, as it is important to determine the amplitudes and directions of the dipole anisotropy in such models. Thus, despite the null results of anisotropy in the simplest pure geometric extension of the ΛCDM model that simultaneously involves anisotropic expansion and spatial curvature, pure geometric generalizations of ΛCDM without touching the underpinning physics deserve further investigations.

REFERENCES

[1] **Akarsu, O.**, **Di Valentino, E.**, **Kumar, S.**, **Ozyigit, M. and Sharma, S.** (2021). Testing spatial curvature and anisotropic expansion on top of the ΛCDM model, `2112.07807`.

[2] **Riess, A.G.** *et al.* (1998). Observational Evidence from Supernovae for an Accelerating Universe and a Cosmological Constant, *The Astronomical Journal*, *116*(3), 1009–1038.

[3] **Perlmutter, S.** *et al.* (1999). Measurements of Ω and Λ from 42 high redshift supernovae, *Astrophysical Journal*, *517*, 565–586.

[4] **Aghanim, N.** *et al.* (2020). Planck 2018 results. VI. Cosmological parameters, *Astronomy & Astrophysics*, *641*, A6.

[5] **Alam, S.** *et al.* (2021). Completed SDSS-IV extended Baryon Oscillation Spectroscopic Survey: Cosmological implications from two decades of spectroscopic surveys at the Apache Point Observatory, *Physical Review D*, *103*(8), 083533.

[6] **Abbott, T.M.C.** *et al.* (2021). Dark Energy Survey Year 3 Results: Cosmological Constraints from Galaxy Clustering and Weak Lensing.

[7] **Di Valentino, E.** *et al.* (2021). Cosmology intertwined III: $f\sigma_8$ and S_8, *Astropart. Phys.*, *131*, 102604.

[8] **Di Valentino, E.** *et al.* (2021). Snowmass2021 - Letter of interest cosmology intertwined IV: The age of the universe and its curvature, *Astropart. Phys.*, *131*, 102607.

[9] **Di Valentino, E.** *et al.* (2021). Snowmass2021 - Letter of interest cosmology intertwined II: The hubble constant tension, *Astropart. Phys.*, *131*, 102605.

[10] **Di Valentino, E.**, **Mena, O.**, **Pan, S.**, **Visinelli, L.**, **Yang, W.**, **Melchiorri, A.**, **Mota, D.F.**, **Riess, A.G. and Silk, J.** (2021). In the realm of the Hubble tension—a review of solutions, *Class. Quant. Grav.*, *38*(15), 153001.

[11] **Perivolaropoulos, L. and Skara, F.** (2021). Challenges for ΛCDM: An update.

[12] **Abdalla, E.** *et al.* (2022). Cosmology intertwined: A review of the particle physics, astrophysics, and cosmology associated with the cosmological tensions and anomalies, *JHEAp*, *34*, 49–211, `2203.06142`.

[13] **Starobinsky, A.A.** (1980). A new type of isotropic cosmological models without singularity, *Phys. Lett. B*, *91*, 99–102.

[14] **Guth, A.H.** (1981). Inflationary universe: A possible solution to the horizon and flatness problems, *Phys. Rev. D*, *23*, 347–356.

[15] **Linde, A.** (1982). A new inflationary universe scenario: A possible solution of the horizon, flatness, homogeneity, isotropy and primordial monopole problems, *Physics Letters B*, *108*(6), 389–393.

[16] **Albrecht, A. and Steinhardt, P.J.** (1982). Cosmology for Grand Unified Theories with Radiatively Induced Symmetry Breaking, *Physical Review Letters*, *48*(17), 1220–1223.

[17] **Linde, A.** (2003). Can we have inflation with Omega > 1?, *Journal of Cosmology and Astroparticle Physics*, *2003*(05), 002–002.

[18] **Efstathiou, G.** (2003). Is the low CMB quadrupole a signature of spatial curvature?, *Mon. Not. Roy. Astron. Soc.*, *343*, L95.

[19] **Handley, W.** (2021). Curvature tension: evidence for a closed universe, *Phys. Rev. D*, *103*(4), L041301.

[20] **Di Valentino, E.**, **Melchiorri, A. and Silk, J.** (2019). Planck evidence for a closed Universe and a possible crisis for cosmology, *Nature Astron.*, *4*(2), 196–203.

[21] **Di Valentino, E.**, **Melchiorri, A. and Silk, J.** (2021). Investigating Cosmic Discordance, *Astrophys. J. Lett.*, *908*(1), L9.

[22] **Vagnozzi, S.**, **Di Valentino, E.**, **Gariazzo, S.**, **Melchiorri, A.**, **Mena, O. and Silk, J.** (2021). The galaxy power spectrum take on spatial curvature and cosmic concordance, *Phys. Dark Univ.*, *33*, 100851.

[23] **Efstathiou, G. and Gratton, S.** (2020). The evidence for a spatially flat Universe, *Mon. Not. Roy. Astron. Soc.*, *496*(1), L91–L95.

[24] **Vagnozzi, S.**, **Loeb, A. and Moresco, M.** (2021). Eppur è piatto? The Cosmic Chronometers Take on Spatial Curvature and Cosmic Concordance, *Astrophys. J.*, *908*(1), 84.

[25] **Acquaviva, G.**, **Akarsu, O.**, **Katirci, N. and Vazquez, J.A.** (2021). Simple-graduated dark energy and spatial curvature, *Phys. Rev. D*, *104*(2), 023505.

[26] **Linde, A.D.** (1995). Inflation with variable Omega, *Phys. Lett. B*, *351*, 99–104.

[27] **Gratton, S.**, **Lewis, A. and Turok, N.** (2002). Closed universes from cosmological instantons, *Phys. Rev. D*, *65*, 043513.

[28] **Uzan, J.P.**, **Kirchner, U. and Ellis, G.F.R.** (2003). WMAP data and the curvature of space, *Mon. Not. Roy. Astron. Soc.*, *344*, L65.

[29] **Collins, C.B.**, **Hawking, S.W. and Sciama, D.W.** (1973). The Rotation and Distortion of the Universe, *Monthly Notices of the Royal Astronomical Society*, *162*(4), 307–320.

[30] **Collins, C.B. and Hawking, S.W.** (1973). Why is the Universe Isotropic?, *Astrophys. J.*, *180*, 317–334.

[31] **Ellis, G.F.R. and van Elst, H.** (1999). Cosmological models: Cargese lectures 1998, *NATO Sci. Ser. C*, *541*, 1–116.

[32] **Ellis, G.**, **Maartens, R. and MacCallum, M.** (2012). *Relativistic cosmology*, Cambridge University Press, United Kingdom.

[33] **Zeldovich, Y.** (1962). The Equation of State at Ultrahigh Densities and Its Relativistic Limitations., *Journal of Experimental and Theoretical Physics*, *14*, 1143.

[34] **Barrow, J.** (1978). Quiescent cosmology, *Nature*, *272*, 211.

[35] **Wald, Robert M.** (1983). Asymptotic behavior of homogeneous cosmological models in the presence of a positive cosmological constant, *Phys. Rev. D*, *28*, 2118–2120.

[36] **Starobinsky A. A.** (1983). Isotropization of arbitrary cosmological expansion given an effective cosmological constant, *JETP Lett.*, *37*, 66.

[37] **Watanabe, M.a.**, **Kanno, S. and Soda, J.** (2009). Inflationary Universe with Anisotropic Hair, *Phys. Rev. Lett.*, *102*, 191302, `0902.2833`.

[38] **Maleknejad, A. and Sheikh-Jabbari, M.M.** (2012). Revisiting Cosmic No-Hair Theorem for Inflationary Settings, *Phys. Rev. D*, *85*, 123508, `1203.0219`.

[39] **Maleknejad, A.**, **Sheikh-Jabbari, M.M. and Soda, J.** (2013). Gauge Fields and Inflation, *Phys. Rept.*, *528*, 161–261, `1212.2921`.

[40] **Barrow, J.D. and Hervik, S.** (2006). Anisotropically inflating universes, *Phys. Rev. D*, *73*, 023007, `gr-qc/0511127`.

[41] **Barrow, J.D. and Hervik, S.** (2010). Simple Types of Anisotropic Inflation, *Phys. Rev. D*, *81*, 023513, `0911.3805`.

[42] **Akarsu, O.**, **Katırcı, N.**, **Özdemir, N. and Vázquez, J.A.** (2020). Anisotropic massive Brans-Dicke gravity extension of the standard ΛCDM model, *Eur. Phys. J. C*, *80*(1), 32, `1903.06679`.

[43] **Mimoso, J.P. and Wands, D.** (1995). Anisotropic scalar - tensor cosmologies, *Phys. Rev. D*, *52*, 5612–5627, `gr-qc/9501039`.

[44] **King, A.R. and Ellis, G.F.R.** (1973). Tilted homogeneous cosmological models, *Commun. Math. Phys.*, *31*, 209–242.

[45] **Goliath, M. and Ellis, G.F.R.** (1999). Homogeneous cosmologies with cosmological constant, *Phys. Rev. D*, *60*, 023502, `gr-qc/9811068`.

[46] **Turner, M.S.** (1991). A Tilted Universe (and Other Remnants of the Preinflationary Universe), *Phys. Rev. D*, *44*, 3737–3748.

[47] **Ellis, G.F.R. and Baldwin, J.E.** (1984). On the expected anisotropy of radio source counts, *Monthly Notices of the Royal Astronomical Society*, *206*(2), 377–381, `https://academic.oup.com/mnras/article-pdf/206/2/377/18187025/mnras206-0377.pdf`.

[48] **Tsagas, C.G.** (2010). Large-scale peculiar motions and cosmic acceleration, *Mon. Not. Roy. Astron. Soc.*, *405*, 503, `0902.3232`.

[49] **Bennett, C.L.**, **Hill, R.S.**, **Hinshaw, G.**, **Larson, D.**, **Smith, K.M.**, **Dunkley, J.**, **Gold, B.**, **Halpern, M.**, **Jarosik, N.**, **Kogut, A.** *et al.* (2011). Seven-year Wilkinson Microwave Anisotropy Probe (WMAP) observations: Are there cosmic microwave background anomalies?, *The Astrophysical Journal Supplement Series*, *192*(2), 17.

[50] **Schwarz, D.J.**, **Copi, C.J.**, **Huterer, D. and Starkman, G.D.** (2016). CMB Anomalies after Planck, *Class. Quant. Grav.*, *33*(18), 184001.

[51] **Akrami, Y.** *et al.* (2020). Planck 2018 results. VII. Isotropy and Statistics of the CMB, *Astron. Astrophys.*, *641*, A7.

[52] **Campanelli, L.**, **Cea, P. and Tedesco, L.** (2006). Ellipsoidal Universe Can Solve The CMB Quadrupole Problem, *Phys. Rev. Lett.*, *97*, 131302.

[53] **Campanelli, L.**, **Cea, P. and Tedesco, L.** (2007). Cosmic Microwave Background Quadrupole and Ellipsoidal Universe, *Phys. Rev. D*, *76*, 063007.

[54] **Koivisto, T. and Mota, D.F.** (2008). Accelerating Cosmologies with an Anisotropic Equation of State, *Astrophys. J.*, *679*, 1–5.

[55] **Rodrigues, D.C.** (2008). Anisotropic Cosmological Constant and the CMB Quadrupole Anomaly, *Phys. Rev. D*, *77*, 023534.

[56] **Koivisto, T. and Mota, D.F.** (2008). Vector Field Models of Inflation and Dark Energy, *JCAP*, *08*, 021.

[57] **Campanelli, Leonardo** (2009). Model of universe anisotropization, *Physical Review D*, *80*(6).

[58] **Koivisto, T. and Mota, D.F.** (2006). Dark energy anisotropic stress and large scale structure formation, *Phys. Rev. D*, *73*, 083502.

[59] **Beltrán Almeida, J.P.**, **Guarnizo, A.**, **Kase, R.**, **Tsujikawa, S. and Valenzuela-Toledo, C.A.** (2019). Anisotropic 2-form dark energy, *Phys. Lett. B*, *793*, 396–404.

[60] **Akarsu, O.**, **Katirci, N.**, **Sen, A.A. and Vazquez, J.A.** (2020). Scalar field emulator via anisotropically deformed vacuum energy: Application to dark energy.

[61] **Akarsu, O.**, **Barrow, J.D. and Uzun, N.M.** (2020). Screening anisotropy via energy-momentum squared gravity: ΛCDM model with hidden anisotropy, *Phys. Rev. D*, *102*(12), 124059.

[62] **Orjuela-Quintana, J.B.**, **Alvarez, M.**, **Valenzuela-Toledo, C.A. and Rodriguez, Y.** (2020). Anisotropic Einstein Yang-Mills Higgs Dark Energy, *JCAP*, *10*, 019.

[63] **Battye, R.A. and Moss, A.** (2006). Anisotropic perturbations due to dark energy, *Phys. Rev. D*, *74*, 041301.

[64] **Koivisto, T. and Mota, D.F.** (2008). Anisotropic Dark Energy: Dynamics of Background and Perturbations, *JCAP*, *06*, 018.

[65] **Cooray, A.R.**, **Holz, D.E. and Caldwell, R.** (2010). Measuring dark energy spatial inhomogeneity with supernova data, *JCAP*, *11*, 015.

[66] **Akarsu, O.**, **Dereli, T. and Oflaz, N.** (2014). Accelerating anisotropic cosmologies in Brans–Dicke gravity coupled to a mass-varying vector field, *Class. Quant. Grav.*, *31*, 045020.

[67] **Chang, Z.**, **Li, M.H.**, **Li, X. and Wang, S.** (2013). Cosmological model with local symmetry of very special relativity and constraints on it from supernovae, *Eur. Phys. J. C*, *73*(6), 2459, `1303.1593`.

[68] **Koivisto, T.S. and Urban, F.R.** (2015). Disformal vectors and anisotropies on a warped brane\protect Hulluilla on Halvat Huvit, *JCAP*, *03*, 003.

[69] **Heisenberg, L.**, **Kase, R. and Tsujikawa, S.** (2016). Anisotropic cosmological solutions in massive vector theories, *JCAP*, *11*, 008.

[70] **Yang, W.**, **Pan, S.**, **Xu, L. and Mota, D.F.** (2019). Effects of anisotropic stress in interacting dark matter – dark energy scenarios, *Mon. Not. Roy. Astron. Soc.*, *482*(2), 1858–1871.

[71] **Pimentel, L.O.** (1989). Energy-momentum tensor in the general scalar-tensor theory, *Classical and Quantum Gravity*, *6*(12), L263–L265.

[72] **Madsen, M.S.** (1988). Scalar fields in curved spacetimes, *Classical and Quantum Gravity*, *5*(4), 627–639.

[73] **Faraoni, V. and Coté, J.** (2018). Imperfect fluid description of modified gravities, *Phys. Rev. D*, *98*(8), 084019.

[74] **Mota, D.F.**, **Kristiansen, J.R.**, **Koivisto, T. and Groeneboom, N.E.** (2007). Constraining Dark Energy Anisotropic Stress, *Mon. Not. Roy. Astron. Soc.*, *382*, 793–800.

[75] **Appleby, S.**, **Battye, R. and Moss, A.** (2010). Constraints on the anisotropy of dark energy, *Physical Review D*, *81*(8).

[76] **Appleby, S.A. and Linder, E.V.** (2013). Probing dark energy anisotropy, *Phys. Rev. D*, *87*(2), 023532.

[77] **Amendola, L.**, **Fogli, S.**, **Guarnizo, A.**, **Kunz, M. and Vollmer, A.** (2014). Model-independent constraints on the cosmological anisotropic stress, *Phys. Rev. D*, *89*(6), 063538.

[78] **Amendola, L.** *et al.* (2018). Cosmology and fundamental physics with the Euclid satellite, *Living Rev. Rel.*, *21*(1), 2.

[79] **Colin, J.**, **Mohayaee, R.**, **Sarkar, S. and Shafieloo, A.** (2011). Probing the anisotropic local Universe and beyond with SNe Ia data, *Mon. Not. Roy. Astron. Soc.*, *414*(2), 264–271.

[80] **Wilczynska, M.R.** *et al.* (2020). Four direct measurements of the fine-structure constant 13 billion years ago, *Sci. Adv.*, *6*(17), eaay9672, `2003.07627`.

[81] **Migkas, K.**, **Schellenberger, G.**, **Reiprich, T.H.**, **Pacaud, F.**, **Ramos-Ceja, M.E. and Lovisari, L.** (2020). Probing cosmic isotropy with a new X-ray galaxy cluster sample through the $L_{\mathrm{X}} - T$ scaling relation, *Astron. Astrophys.*, *636*, A15, `2004.03305`.

[82] **Chang, Z.**, **Lin, H.N.**, **Sang, Y. and Wang, S.** (2018). A tomographic test of cosmological principle using the JLA compilation of type Ia supernovae, *Mon. Not. Roy. Astron. Soc.*, *478*(3), 3633–3639, `1711.11321`.

[83] **Secrest, N.J.**, **von Hausegger, S.**, **Rameez, M.**, **Mohayaee, R.**, **Sarkar, S. and Colin, J.** (2021). A Test of the Cosmological Principle with Quasars, *Astrophys. J. Lett.*, *908*(2), L51, `2009.14826`.

[84] **Siewert, T.M.**, **Schmidt-Rubart, M. and Schwarz, D.J.** (2021). Cosmic radio dipole: Estimators and frequency dependence, *Astron. Astrophys.*, *653*, A9, `2010.08366`.

[85] **Migkas, K.**, **Pacaud, F.**, **Schellenberger, G.**, **Erler, J.**, **Nguyen-Dang, N.T.**, **Reiprich, T.H.**, **Ramos-Ceja, M.E. and Lovisari, L.** (2021). Cosmological implications of the anisotropy of ten galaxy cluster scaling relations, *Astron. Astrophys.*, *649*, A151, `2103.13904`.

[86] **Rahman, W.**, **Trotta, R.**, **Boruah, S.S.**, **Hudson, M.J. and van Dyk, D.A.** (2021). New Constraints on Anisotropic Expansion from Supernovae Type Ia, `2108.12497`.

[87] **Heinesen, A. and Macpherson, H.J.** (2022). A prediction for anisotropies in the nearby Hubble flow, *JCAP*, *03*(03), 057, `2111.14423`.

[88] **Park, C.G. and Ratra, B.** (2019). Using the tilted flat-ΛCDM and the untilted non-flat ΛCDM inflation models to measure cosmological parameters from a compilation of observational data, *Astrophys. J.*, *882*, 158, `1801.00213`.

[89] **Park, C.G. and Ratra, B.** (2020). Using SPT polarization, *Planck* 2015, and non-CMB data to constrain tilted spatially-flat and untilted nonflat ΛCDM , XCDM, and ϕCDM dark energy inflation cosmologies, *Phys. Rev. D*, *101*(8), 083508, `1908.08477`.

[90] **Macpherson, H.J. and Heinesen, A.** (2021). Luminosity distance and anisotropic sky-sampling at low redshifts: A numerical relativity study, *Phys. Rev. D*, *104*, 023525, [Erratum: Phys.Rev.D 104, 109901 (2021)], `2103.11918`.

[91] **Yeung, S. and Chu, M.C.** (2022). Directional variations of cosmological parameters from the Planck CMB data, *Phys. Rev. D*, *105*(8), 083508, `2201.03799`.

[92] **Krishnan, C.**, **Mohayaee, R.**, **Colgáin, E.O.**, **Sheikh-Jabbari, M.M. and Yin, L.** (2021). Does Hubble tension signal a breakdown in FLRW cosmology?, *Class. Quant. Grav.*, *38*(18), 184001, `2105.09790`.

[93] **Krishnan, C.**, **Mohayaee, R.**, **Colgáin, E.O.**, **Sheikh-Jabbari, M.M. and Yin, L.** (2022). Hints of FLRW breakdown from supernovae, *Phys. Rev. D*, *105*(6), 063514, `2106.02532`.

[94] **Luongo, O.**, **Muccino, M.**, **Colgáin, E.O.**, **Sheikh-Jabbari, M.M. and Yin, L.** (2022). Larger H0 values in the CMB dipole direction, *Phys. Rev. D*, *105*(10), 103510, `2108.13228`.

[95] **Cea, P.** (2022). The Ellipsoidal Universe and the Hubble tension, `2201.04548`.

[96] **Camarena, D.**, **Marra, V.**, **Sakr, Z. and Clarkson, C.** (2022). A void in the Hubble tension? The end of the line for the Hubble bubble, `2205.05422`.

[97] **Tsagas, C.G.** (2011). Peculiar motions, accelerated expansion and the cosmological axis, *Phys. Rev. D*, *84*, 063503, `1107.4045`.

[98] **Tsagas, C.G. and Kadiltzoglou, M.I.** (2015). Deceleration parameter in tilted Friedmann universes, *Phys. Rev. D*, *92*(4), 043515, `1507.04266`.

[99] **Colin, J.**, **Mohayaee, R.**, **Rameez, M. and Sarkar, S.** (2019). Evidence for anisotropy of cosmic acceleration, *Astron. Astrophys.*, *631*, L13, `1808.04597`.

[100] **Asvesta, K.**, **Kazantzidis, L.**, **Perivolaropoulos, L. and Tsagas, C.G.** (2022). Observational constraints on the deceleration parameter in a tilted universe, `2202.00962`.

[101] **Lin, H.N.**, **Wang, S.**, **Chang, Z. and Li, X.** (2016). Testing the isotropy of the Universe by using the JLA compilation of type-Ia supernovae, *Mon. Not. Roy. Astron. Soc.*, *456*(2), 1881–1885, `1504.03428`.

[102] **Li, X.**, **Lin, H.N.**, **Wang, S. and Chang, Z.** (2015). A unified description for dipoles of the fine-structure constant and SnIa Hubble diagram in Finslerian universe, *Eur. Phys. J. C*, *75*(5), 181, `1501.06738`.

[103] **Akarsu, O.**, **Kumar, S.**, **Sharma, S. and Tedesco, L.** (2019). Constraints on a Bianchi type I spacetime extension of the standard ΛCDM model, *Phys. Rev. D*, *100*(2), 023532.

[104] **Riess, A.G.** *et al.* (2021). A Comprehensive Measurement of the Local Value of the Hubble Constant with 1 km/s/Mpc Uncertainty from the Hubble Space Telescope and the SH0ES Team.

[105] **Freedman, W.L.** *et al.* (2019). The Carnegie-Chicago Hubble Program. VIII. An Independent Determination of the Hubble Constant Based on the Tip of the Red Giant Branch.

[106] **Riess, A.G.**, **Casertano, S.**, **Yuan, W.**, **Bowers, J.B.**, **Macri, L.**, **Zinn, J.C. and Scolnic, D.** (2021). Cosmic Distances Calibrated to 1% Precision with Gaia EDR3 Parallaxes and Hubble Space Telescope Photometry of 75 Milky Way Cepheids Confirm Tension with ΛCDM, *Astrophys. J. Lett.*, *908*(1), L6.

[107] **Campanelli, L.**, **Cea, P.**, **Fogli, G.L. and Marrone, A.** (2011). Testing the Isotropy of the Universe with Type Ia Supernovae, *Phys. Rev. D*, *83*, 103503.

[108] **Wang, Y.Y. and Wang, F.Y.** (2018). Testing the isotropy of the Universe with type Ia supernovae in a model-independent way, *Mon. Not. Roy. Astron. Soc.*, *474*(3), 3516–3522.

[109] **Beltran Jimenez, J.**, **Salzano, V. and Lazkoz, R.** (2015). Anisotropic expansion and SNIa: an open issue, *Phys. Lett. B*, *741*, 168–177.

[110] **Soltis, J.**, **Farahi, A.**, **Huterer, D. and Liberato, C.M.** (2019). Percent-Level Test of Isotropic Expansion Using Type Ia Supernovae, *Phys. Rev. Lett.*, *122*(9), 091301.

[111] **Zhao, D.**, **Zhou, Y. and Chang, Z.** (2019). Anisotropy of the Universe via the Pantheon supernovae sample revisited, *Mon. Not. Roy. Astron. Soc.*, *486*(4), 5679–5689.

[112] **Hu, J.P.**, **Wang, Y.Y. and Wang, F.Y.** (2020). Testing cosmic anisotropy with Pantheon sample and quasars at high redshifts, *Astron. Astrophys.*, *643*, A93.

[113] **Kalus, B.**, **Schwarz, D.J.**, **Seikel, M. and Wiegand, A.** (2013). Constraints on anisotropic cosmic expansion from supernovae, *Astron. Astrophys.*, *553*, A56.

[114] **Amirhashchi, H. and Amirhashchi, S.** (2020). Constraining Bianchi Type I Universe With Type Ia Supernova and H(z) Data, *Phys. Dark Univ.*, *29*, 100557, `1802.04251`.

[115] **Martinez-Gonzalez, E. and Sanz, J.L.** (1995). {DELTA}T/T and the isotropy of the universe., *Astronomy and Astrophysics*, *300*, 346.

[116] **Bunn, E.F.**, **Ferreira, P. and Silk, J.** (1996). How anisotropic is our universe?, *Phys. Rev. Lett.*, *77*, 2883–2886.

[117] **Kogut, A.**, **Hinshaw, G. and Banday, A.J.** (1997). Limits to global rotation and shear from the COBE DMR four year sky maps, *Phys. Rev. D*, *55*, 1901–1905.

[118] **Barrow, J.D.** (1997). Cosmological limits on slightly skew stresses, *Phys. Rev. D*, *55*, 7451–7460.

[119] **Saadeh, D.**, **Feeney, S.M.**, **Pontzen, A.**, **Peiris, H.V. and McEwen, J.D.** (2016). How Isotropic is the Universe?, *Physical Review Letters*, *117*, 131302.

[120] **Pontzen, A.**, http://www.scholarpedia.org/article/Bianchi_universes.

[121] **Saadeh, D.**, **Feeney, S.M.**, **Pontzen, A.**, **Peiris, H.V. and McEwen, J.D.** (2016). A framework for testing isotropy with the cosmic microwave background, *Mon. Not. Roy. Astron. Soc.*, *462*(2), 1802–1811.

[122] **Barrow, J.** (1976). Light elements and the isotropy of the Universe, *Monthly Notices of the Royal Astronomical Society*, *175*, 359–370.

[123] **Campanelli, L.** (2011). Helium-4 synthesis in an anisotropic universe, *Phys. Rev. D*, *84*, 123521.

[124] **Fixsen, D.J.** (2009). The Temperature of the Cosmic Microwave Background, *Astrophys. J.*, *707*, 916–920.

[125] **Hu, W.** (1998). Structure formation with generalized dark matter, *Astrophys. J.*, *506*, 485–494, astro-ph/9801234.

[126] **Battefeld, T.J. and Easson, D.A.** (2004). Perturbations in a holographic universe and in other stiff fluid cosmologies, *Phys. Rev. D*, *70*, 103516, hep-th/0408154.

[127] **Chavanis, P.H.** (2015). Cosmology with a stiff matter era, *Phys. Rev. D*, *92*(10), 103004.

[128] **Copeland, E.J.**, **Liddle, A.R. and Wands, D.** (1998). Exponential potentials and cosmological scaling solutions, *Phys. Rev. D*, *57*, 4686–4690, gr-qc/9711068.

[129] **Tamanini, N.** (2014). Dynamics of cosmological scalar fields, *Phys. Rev. D*, *89*, 083521, 1401.6339.

[130] **Odintsov, S.D. and Oikonomou, V.K.** (2017). Early-time cosmology with stiff era from modified gravity, *Phys. Rev. D*, *96*(10), 104059, 1711.04571.

[131] **Poulin, V.**, **Smith, T.L.**, **Karwal, T. and Kamionkowski, M.** (2019). Early Dark Energy Can Resolve The Hubble Tension, *Phys. Rev. Lett.*, *122*(22), 221301, 1811.04083.

[132] **Jiang, J.Q. and Piao, Y.S.** (2022). Toward early dark energy and ns=1 with Planck, ACT, and SPT observations, *Phys. Rev. D*, *105*(10), 103514, 2202.13379.

[133] **Mavromatos, N.E. and Solà Peracaula, J.** (2021). Stringy-running-vacuum-model inflation: from primordial gravitational waves and stiff axion matter to dynamical dark energy, *Eur. Phys. J. ST*, *230*(9), 2077–2110, 2012.07971.

[134] **Banks, T. and Fischler, W.** (2001). An Holographic cosmology, `hep-th/0111142`.

[135] **Banks, T. and Fischler, W.** (2005). Holographic cosmology 3.0, *Phys. Scripta T*, *117*, 56–63, `hep-th/0310288`.

[136] **Banks, T.**, **Fischler, W. and Mannelli, L.** (2005). Microscopic quantum mechanics of the p = rho universe, *Phys. Rev. D*, *71*, 123514, `hep-th/0408076`.

[137] **Mimoso, J.P. and Wands, D.** (1995). Massless fields in scalar - tensor cosmologies, *Phys. Rev. D*, *51*, 477–489, `gr-qc/9405025`.

[138] **Chavanis, P.H.** (2015). Partially relativistic self-gravitating Bose-Einstein condensates with a stiff equation of state, *Eur. Phys. J. Plus*, *130*, 181, `1412.0005`.

[139] **Andersson, L. and Rendall, A.D.** (2001). Quiescent cosmological singularities, *Commun. Math. Phys.*, *218*, 479–511, `gr-qc/0001047`.

[140] **Lankinen, J. and Vilja, I.** (2017). Gravitational Particle Creation in a Stiff Matter Dominated Universe, *JCAP*, *08*, 025, `1612.02586`.

[141] **Easson, D.A.**, **Manton, T. and Svesko, A.** (2021). Cosmic acceleration from string induced Galileons, *JCAP*, *10*, 076, `2107.00020`.

[142] **Benisty, D.**, **Guendelman, E.I.**, **van de Venn, A.**, **Vasak, D.**, **Struckmeier, J. and Stoecker, H.** (2022). The dark side of the torsion: dark energy from propagating torsion, *Eur. Phys. J. C*, *82*(3), 264, `2109.01052`.

[143] **Akarsu, O.**, **Barrow, J.D.**, **Çıkıntoğlu, S.**, **Ekşi, K.Y. and Katırcı, N.** (2018). Constraint on energy-momentum squared gravity from neutron stars and its cosmological implications, *Phys. Rev. D*, *97*(12), 124017.

[144] **Dutta, J.**, **Khyllep, W.**, **Saridakis, E.N.**, **Tamanini, N. and Vagnozzi, S.** (2018). Cosmological dynamics of mimetic gravity, *JCAP*, *02*, 041, `1711.07290`.

[145] **Benisty, D.**, **Chaichian, M. and Oksanen, M.** (2021). Mimetic Tensor-Vector-Scalar Cosmology: Unified Dark Energy, Dark Matter and Stiff Matter.

[146] **Cramer, J.G.**, **Forward, R.L.**, **Morris, M.S.**, **Visser, M.**, **Benford, G. and Landis, G.A.** (1995). Natural wormholes as gravitational lenses, *Phys. Rev. D*, *51*, 3117–3120, `astro-ph/9409051`.

[147] **Pereira, T.S.**, **Pitrou, C. and Uzan, J.P.** (2007). Theory of cosmological perturbations in an anisotropic universe, *JCAP*, *09*, 006, `0707.0736`.

[148] **Ade, P.A.R.** *et al.* (2014). Planck 2013 results. XV. CMB power spectra and likelihood, *Astron. Astrophys.*, *571*, A15, `1303.5075`.

[149] **Jimenez, R. and Loeb, A.** (2002). Constraining cosmological parameters based on relative galaxy ages, *Astrophys. J.*, *573*, 37–42.

[150] **Scolnic, D.M.** *et al.* (2018). The Complete Light-curve Sample of Spectroscopically Confirmed SNe Ia from Pan-STARRS1 and Cosmological Constraints from the Combined Pantheon Sample, *Astrophys. J.*, *859*(2), 101.

[151] **Sharma, S.** (2020). Probing phenomenological emergent dark energy model in a Bianchi type-I spacetime with the recent observational data, *Phys. Dark Univ.*, *30*, 100717.

[152] **Betoule, M.** *et al.* (2014). Improved cosmological constraints from a joint analysis of the SDSS-II and SNLS supernova samples, *Astron. Astrophys.*, *568*, A22.

[153] **Conley, A.** *et al.* (2011). Supernova Constraints and Systematic Uncertainties from the First Three Years of the Supernova Legacy Survey, *The Astrophysical Journal Supplement Series*, *192*(1), 1.

[154] **Alam, S.** *et al.* (2021). Completed SDSS-IV extended Baryon Oscillation Spectroscopic Survey: Cosmological implications from two decades of spectroscopic surveys at the Apache Point Observatory, *Phys. Rev. D*, *103*(8), 083533.

[155] **2018 Cosmological parameters and MC chains**, `https://wiki.cosmos.esa.int/planck-legacy-archive/index.php/Cosmological_Parameters`.

[156] **Cooke, R.J.**, **Pettini, M.**, **Nollett, K.M. and Jorgenson, R.** (2016). The primordial deuterium abundance of the most metal-poor damped Lyα system, *Astrophys. J.*, *830*(2), 148.

[157] **Mangano, G.**, **Miele, G.**, **Pastor, S.**, **Pinto, T.**, **Pisanti, O. and Serpico, P.D.** (2005). Relic neutrino decoupling including flavor oscillations, *Nucl. Phys. B*, *729*, 221–234.

[158] **de Salas, P.F. and Pastor, S.** (2016). Relic neutrino decoupling with flavour oscillations revisited, *JCAP*, *07*, 051.

[159] **Akita, K. and Yamaguchi, M.** (2020). A precision calculation of relic neutrino decoupling, *JCAP*, *08*, 012.

[160] **Froustey, J.**, **Pitrou, C. and Volpe, M.C.** (2020). Neutrino decoupling including flavour oscillations and primordial nucleosynthesis, *JCAP*, *12*, 015.

[161] **Bennett, J.J.**, **Buldgen, G.**, **De Salas, P.F.**, **Drewes, M.**, **Gariazzo, S.**, **Pastor, S. and Wong, Y.Y.Y.** (2021). Towards a precision calculation of $N_{\rm eff}$ in the Standard Model II: Neutrino decoupling in the presence of flavour oscillations and finite-temperature QED, *JCAP*, *04*, 073.

[162] **Aubourg, E.** *et al.* (2015). Cosmological implications of baryon acoustic oscillation measurements, *Phys. Rev. D*, *92*(12), 123516.

[163] **Feroz, F. and Hobson, M.P.** (2008). Multimodal nested sampling: an efficient and robust alternative to MCMC methods for astronomical data analysis, *Mon. Not. Roy. Astron. Soc.*, *384*, 449.

[164] **Feroz, F.**, **Hobson, M.P. and Bridges, M.** (2009). MultiNest: an efficient and robust Bayesian inference tool for cosmology and particle physics, *Mon. Not. Roy. Astron. Soc.*, *398*, 1601–1614.

[165] **Feroz, F.**, **Hobson, M.P.**, **Cameron, E. and Pettitt, A.N.** (2019). Importance Nested Sampling and the MultiNest Algorithm, *Open J. Astrophys.*, *2*(1), 10.

[166] **Buchner, J.**, **Georgakakis, A.**, **Nandra, K.**, **Hsu, L.**, **Rangel, C.**, **Brightman, M.**, **Merloni, A.**, **Salvato, M.**, **Donley, J. and Kocevski, D.** (2014). X-ray spectral modelling of the AGN obscuring region in the CDFS: Bayesian model selection and catalogue, *Astron. Astrophys.*, *564*, A125.

[167] **Skilling, J.** (2004). Nested Sampling, *AIP Conference Proceedings*, *735*(1), 395–405.

[168] **Kass, R.E. and Raftery, A.E.** (1995). Bayes Factors, *Journal of the American Statistical Association*, *90*(430), 773–795.

APPENDICES

APPENDIX A : Robertson-Walker metric
APPENDIX B : Bianchi type I metric
APPENDIX C : Bianchi type V metric
APPENDIX D : Bianchi type IX metric

APPENDIX A

We consider Robertson-Walker metric in the form,

$$\mathrm{d}s^2 = -\mathrm{d}t^2 + s^2 \frac{\mathrm{d}x^2 + \mathrm{d}y^2 + \mathrm{d}z^2}{\left[1 + \frac{\kappa}{4}(x^2 + y^2 + z^2)\right]^2}. \tag{A.1}$$

Non-zero components of Christoffel Symbols written as,

$$\begin{aligned}
&\Gamma^0_{11} = \Gamma^0_{22} = \Gamma^0_{33} = \frac{16\dot{s}s}{[4 + \kappa(x^2 + y^2 + z^2)]^2}, \quad \Gamma^1_{01} = \Gamma^2_{02} = \Gamma^3_{03} = \frac{\dot{s}}{s},\\
&\Gamma^3_{13} = \Gamma^2_{12} = \Gamma^1_{11} = -\frac{2\kappa x}{4 + \kappa(x^2 + y^2 + z^2)}, \quad \Gamma^1_{33} = \Gamma^1_{22} = \frac{2\kappa x}{4 + \kappa(x^2 + y^2 + z^2)},\\
&\Gamma^1_{12} = \Gamma^3_{23} = \Gamma^2_{22} = -\frac{2\kappa y}{4 + \kappa(x^2 + y^2 + z^2)}, \quad \Gamma^2_{11} = \Gamma^2_{33} = \frac{2\kappa y}{4 + \kappa(x^2 + y^2 + z^2)},\\
&\Gamma^1_{13} = \Gamma^2_{23} = \Gamma^3_{33} = -\frac{2\kappa z}{4 + \kappa(x^2 + y^2 + z^2)} \quad \Gamma^3_{11} = \Gamma^3_{22} = \frac{2\kappa z}{4 + \kappa(x^2 + y^2 + z^2)}.
\end{aligned} \tag{A.2}$$

Non-zero components of Ricci tensor written as,

$$R_{00} = -3\frac{\ddot{s}}{s}, \tag{A.3}$$

$$R_{11} = R_{22} = R_{33} = \frac{\ddot{s}s + 2\dot{s}^2 + 2\kappa}{\left[1 + \frac{\kappa}{4}(x^2 + y^2 + z^2)\right]^2}. \tag{A.4}$$

Ricci scalar yields,

$$R = 6\left(\frac{\ddot{s}}{s} + \frac{\dot{s}^2}{s^2} + \frac{\kappa}{s^2}\right). \tag{A.5}$$

Within the framework of the metric given by (A.1), Einstein field equations read as,

$$G_{00} = 3\frac{\dot{s}^2}{s^2} + 3\frac{\kappa}{s^2} = 8\pi G T_{00}, \tag{A.6}$$

$$G_{11} = \frac{2\ddot{s}s + \dot{s}^2 + \kappa}{\left[1 + \frac{\kappa}{4}(x^2 + y^2 + z^2)\right]^2} = 8\pi G T_{11}, \tag{A.7}$$

$$G_{22} = \frac{2\ddot{s}s + \dot{s}^2 + \kappa}{\left[1 + \frac{\kappa}{4}(x^2 + y^2 + z^2)\right]^2} = 8\pi G T_{22}, \tag{A.8}$$

$$G_{33} = \frac{2\ddot{s}s + \dot{s}^2 + \kappa}{\left[1 + \frac{\kappa}{4}(x^2 + y^2 + z^2)\right]^2} = 8\pi G T_{33}. \tag{A.9}$$

APPENDIX B

We consider Bianchi type I metric in the form,

$$\mathrm{d}s^2 = -\mathrm{d}t^2 + a^2\mathrm{d}x^2 + b^2\mathrm{d}y^2 + c^2\mathrm{d}z^2. \tag{B.1}$$

Non-zero components of Christoffel Symbols written as,

$$\begin{aligned} \Gamma^0_{11} &= a\dot{a}, \quad \Gamma^1_{01} = \frac{\dot{a}}{a}, \\ \Gamma^0_{22} &= b\dot{b}, \quad \Gamma^2_{02} = \frac{\dot{b}}{b}, \\ \Gamma^0_{33} &= c\dot{c}, \quad \Gamma^3_{03} = \frac{\dot{c}}{c}. \end{aligned} \tag{B.2}$$

Non-zero components of Ricci tensor written as,

$$R_{00} = -\frac{\ddot{a}}{a} - \frac{\ddot{b}}{b} - \frac{\ddot{c}}{c}, \tag{B.3}$$

$$R_{11} = a\left(\ddot{a} + \frac{\dot{a}\dot{c}}{c} + \frac{\dot{a}\dot{b}}{b}\right), \tag{B.4}$$

$$R_{22} = b\left(\ddot{b} + \frac{\dot{b}\dot{c}}{c} + \frac{\dot{a}\dot{b}}{a}\right), \tag{B.5}$$

$$R_{33} = c\left(\ddot{c} + \frac{\dot{b}\dot{c}}{b} + \frac{\dot{a}\dot{c}}{a}\right). \tag{B.6}$$

Ricci scalar yields,

$$R = 2\left(\frac{\dot{a}}{a}\frac{\dot{b}}{b} + \frac{\dot{a}}{a}\frac{\dot{c}}{c} + \frac{\dot{b}}{b}\frac{\dot{c}}{c} - \frac{\ddot{a}}{a} + \frac{\ddot{b}}{b} + \frac{\ddot{c}}{c}\right). \tag{B.7}$$

Within the framework of the metric given by (B.1), Einstein field equations read as,

$$G_{00} = \frac{\dot{a}}{a}\frac{\dot{b}}{b} + \frac{\dot{b}}{b}\frac{\dot{c}}{c} + \frac{\dot{a}}{a}\frac{\dot{c}}{c} = 8\pi G T_{00}, \tag{B.8}$$

$$G_{11} = -a^2\left(\frac{\ddot{b}}{b} + \frac{\ddot{c}}{c} + \frac{\dot{b}}{b}\frac{\dot{c}}{c}\right) = 8\pi G T_{11}, \tag{B.9}$$

$$G_{22} = -b^2\left(\frac{\ddot{a}}{a} + \frac{\ddot{c}}{c} + \frac{\dot{a}}{a}\frac{\dot{c}}{c}\right) = 8\pi G T_{22}, \tag{B.10}$$

$$G_{33} = -c^2\left(\frac{\ddot{a}}{a} + \frac{\ddot{b}}{b} + \frac{\dot{a}}{a}\frac{\dot{b}}{b}\right) = 8\pi G T_{33}. \tag{B.11}$$

APPENDIX C

We consider Bianchi type V metric in the form,

$$\mathrm{d}s^2 = -\mathrm{d}t^2 + a^2 e^{-2mz}\mathrm{d}x^2 + b^2 e^{-2mz}\mathrm{d}y^2 + c^2\mathrm{d}z^2. \tag{C.1}$$

Non-zero components of Christoffel Symbols written as,

$$\begin{aligned}
&\Gamma^0_{11} = a\dot{a}e^{-2mz}, \quad \Gamma^1_{01} = \frac{\dot{a}}{a},\\
&\Gamma^0_{22} = b\dot{b}e^{-2mz}, \quad \Gamma^2_{02} = \frac{\dot{b}}{b},\\
&\Gamma^0_{33} = c\dot{c}, \qquad\qquad \Gamma^3_{03} = \frac{\dot{c}}{c},\\
&\Gamma^3_{22} = \Gamma^3_{11} = m, \quad \Gamma^1_{13} = \Gamma^2_{23} = -m.
\end{aligned} \tag{C.2}$$

Non-zero components of Ricci tensor written as,

$$R_{00} = -\frac{\ddot{a}}{a} - \frac{\ddot{b}}{b} - \frac{\ddot{c}}{c}, \tag{C.3}$$

$$R_{11} = ae^{-2mz}\left(\ddot{a} + \frac{\dot{a}\dot{c}}{c} + \frac{\dot{a}\dot{b}}{b} - \frac{2m^2 a}{c^2}\right), \tag{C.4}$$

$$R_{22} = be^{-2mz}\left(\ddot{b} + \frac{\dot{b}\dot{c}}{c} + \frac{\dot{a}\dot{b}}{a} - \frac{2m^2 b}{c^2}\right), \tag{C.5}$$

$$R_{33} = c\left(\ddot{c} + \frac{\dot{b}\dot{c}}{b} + \frac{\dot{a}\dot{c}}{a} - \frac{2m^2}{c}\right), \tag{C.6}$$

$$R_{03} = -m\left(2\frac{\dot{c}}{c} - \frac{\dot{a}}{a} - \frac{\dot{b}}{b}\right). \tag{C.7}$$

Ricci scalar yields,

$$R = 2\left(\frac{\dot{a}}{a}\frac{\dot{b}}{b} + \frac{\dot{a}}{a}\frac{\dot{c}}{c} + \frac{\dot{b}}{b}\frac{\dot{c}}{c} - \frac{\ddot{a}}{a} + \frac{\ddot{b}}{b} + \frac{\ddot{c}}{c} - 3\frac{m^2}{c^2}\right). \tag{C.8}$$

Within the framework of the metric given by (C.1), Einstein field equations read as,

$$G_{00} = \frac{\dot{a}}{a}\frac{\dot{b}}{b} + \frac{\dot{b}}{b}\frac{\dot{c}}{c} + \frac{\dot{a}}{a}\frac{\dot{c}}{c} - 3\frac{m^2}{c^2} = 8\pi G T_{00}, \tag{C.9}$$

$$G_{11} = -a^2 e^{2mz}\left(\frac{\ddot{b}}{b} + \frac{\ddot{c}}{c} + \frac{\dot{b}}{b}\frac{\dot{c}}{c} - \frac{m^2}{c^2}\right) = 8\pi G T_{11}, \tag{C.10}$$

$$G_{22} = -b^2 e^{2mz}\left(\frac{\ddot{a}}{a} + \frac{\ddot{c}}{c} + \frac{\dot{a}}{a}\frac{\dot{c}}{c} - \frac{m^2}{c^2}\right) = 8\pi G T_{22}, \tag{C.11}$$

$$G_{33} = -c^2\left(\frac{\ddot{a}}{a} + \frac{\ddot{b}}{b} + \frac{\dot{a}}{a}\frac{\dot{b}}{b} - \frac{m^2}{c^2}\right) = 8\pi G T_{33}, \tag{C.12}$$

$$G_{03} = -m\left(2\frac{\dot{c}}{c} - \frac{\dot{a}}{a} - \frac{\dot{b}}{b}\right) = 8\pi G T_{03}. \tag{C.13}$$

APPENDIX D

We consider Bianchi type IX metric in the form,

$$\begin{aligned} \mathrm{d}s^2 = &-\mathrm{d}t^2 + a^2\mathrm{d}x^2 + b^2\mathrm{d}y^2 \\ &+ \left(b^2\sin^2 2ny + a^2\cos^2 2ny\right)\mathrm{d}z^2 - 2a^2\cos 2ny\,\mathrm{d}x\mathrm{d}z. \end{aligned} \tag{D.1}$$

Non-zero components of Christoffel Symbols written as,

$$\begin{aligned}
&\Gamma^0_{11} = a\dot{a}, && \Gamma^0_{22} = b\dot{b}, \\
&\Gamma^1_{01} = \frac{\dot{a}}{a}, && \Gamma^2_{13} = -\frac{a^2}{b^2}n\sin 2ny, \\
&\Gamma^1_{03} = \left(\frac{\dot{b}}{b} - \frac{\dot{a}}{a}\right)\cos 2ny, && \Gamma^0_{13} = -a\dot{a}\cos 2ny, \\
&\Gamma^2_{02} = \Gamma^3_{03} = \frac{\dot{b}}{b}, && \Gamma^3_{23} = -\frac{n\cos 2ny(-2b^2 + a^2)}{b^2\sin 2ny}, \\
&\Gamma^2_{33} = -2n\sin 2ny\cos 2ny\left(1 - \frac{a^2}{b^2}\right), && \Gamma^3_{21} = \frac{a^2 n}{b^2\sin 2ny}, \\
&\Gamma^1_{12} = \frac{a^2 n\cos 2ny}{b^2\sin 2ny}, && \Gamma^0_{33} = b\dot{b}\sin^2 2ny + a\dot{a}\cos^2 2ny, \\
&\Gamma^1_{23} = -\frac{[(a^2 - b^2)\cos^2 2ny - b^2]n}{b^2\sin 2ny}.
\end{aligned} \tag{D.2}$$

Non-zero components of Ricci tensor written as,

$$R_{00} = -\frac{\ddot{a}}{a} - \frac{\ddot{b}}{b}, \tag{D.3}$$

$$R_{11} = a\left(\ddot{a} + 2\frac{\dot{a}\dot{b}}{b} + 2n^2\frac{a^3}{b^4}\right), \tag{D.4}$$

$$R_{22} = b\frac{\dot{a}\dot{b}}{a} + b\ddot{b} + \dot{b}^2 + 4n^2 - 2n^2\frac{a^2}{b^2}, \tag{D.5}$$

$$\begin{aligned} R_{33} = \cos^2 2ny &\left(-b\frac{\dot{a}\dot{b}}{a} - b\ddot{b} - \dot{b}^2 + a\ddot{a} - 4n^2 2\frac{\dot{a}\dot{b}}{ab} + 2n^2\frac{a^2}{b^2} + 2n^2\frac{a^4}{b^4}\right) \\ &+ b\frac{\dot{a}\dot{b}}{a} + b\ddot{b} + \dot{b}^2 + 4n^2 - 2n^2\frac{a^2}{b^4}, \end{aligned} \tag{D.6}$$

$$R_{13} = -a\cos 2ny\left(\ddot{a} + 2\frac{\dot{a}\dot{b}}{b} + 2n^2\frac{a^3}{b^4}\right). \tag{D.7}$$

Ricci scalar yields,

$$R = 2\left(2\frac{\ddot{b}}{b} - \frac{a^2n^2}{b^4} + \frac{\dot{b}^2}{b^2} + 4\frac{n^2}{b^2} + 2\frac{\dot{a}\dot{b}}{ab}\right). \tag{D.8}$$

Within the framework of the metric given by (D.1), Einstein field equations read as,

$$G_{00} = 2\frac{\dot{a}\dot{b}}{ab} + \frac{\dot{b}^2}{b^2} + \frac{1}{b^2} - \frac{1}{4}\frac{a^2}{b^4} = 8\pi G T_{00}, \tag{D.9}$$

$$G_{11} = -a^2\left(2\frac{\ddot{b}}{b} + \frac{\dot{b}^2}{b^2} + \frac{1}{b^2} - \frac{3}{4}\frac{a^2}{b^4}\right) = 8\pi G T_{11}, \tag{D.10}$$

$$G_{22} = -b^2\left(\frac{\ddot{a}}{a} + \frac{\ddot{b}}{b} + \frac{\dot{a}\dot{b}}{ab} + \frac{1}{4}\frac{a^2}{b^4}\right) = 8\pi G T_{22}, \tag{D.11}$$

$$\begin{aligned} G_{33} = \cos^2 y \Bigg(& b^2\frac{\ddot{a}}{a} + b\ddot{b} + \dot{a}\dot{b}\frac{b}{a} \\ & -2a^2\frac{\ddot{b}}{b} - a^2\frac{\dot{b}^2}{b^2} - \frac{3}{4}\frac{a^2}{b^2} + \frac{3}{4}\frac{a^4}{b^4}\Bigg) \\ & - b^2\left(\frac{\ddot{a}}{a} + \frac{\ddot{b}}{b} + \frac{\dot{a}\dot{b}}{ab} + \frac{1}{4}\frac{a^2}{b^4}\right) = 8\pi G T_{33}, \end{aligned} \tag{D.12}$$

$$G_{13} = a^2 \cos y \left(2\frac{\dot{a}\dot{b}}{ab} + \frac{\dot{b}^2}{b^2} + \frac{1}{b^2} - \frac{1}{4}\frac{a^2}{b^4}\right) = 8\pi G T_{13}. \tag{D.13}$$

CURRICULUM VITAE

Name Surname : Maya Özyiğit

EDUCATION :

- **B.Sc.** : 2019, Istanbul Technical University, Faculty of Science and Letters, Department of Physics Engineering

PUBLICATIONS, PRESENTATIONS AND PATENTS ON THE THESIS:

- **Özyiğit M.** 2022. Anisotropic and Curvature Generalization of ΛCDM Model. *Turkish Physical Society* 38^{th} *International Physics Congress*, August 31 – September 4, 2022 Bodrum, Turkey.

M. Özyiğit

TESTING SPATIAL CURVATURE AND ANISOTROPIC EXPANSION
OF THE UNIVERSE ON TOP OF THE ΛCDM MODEL

2022